REPORT –

Development of a Hydrogeologic Framework for Atascosa County Based on the Analysis of Geophysical Logs

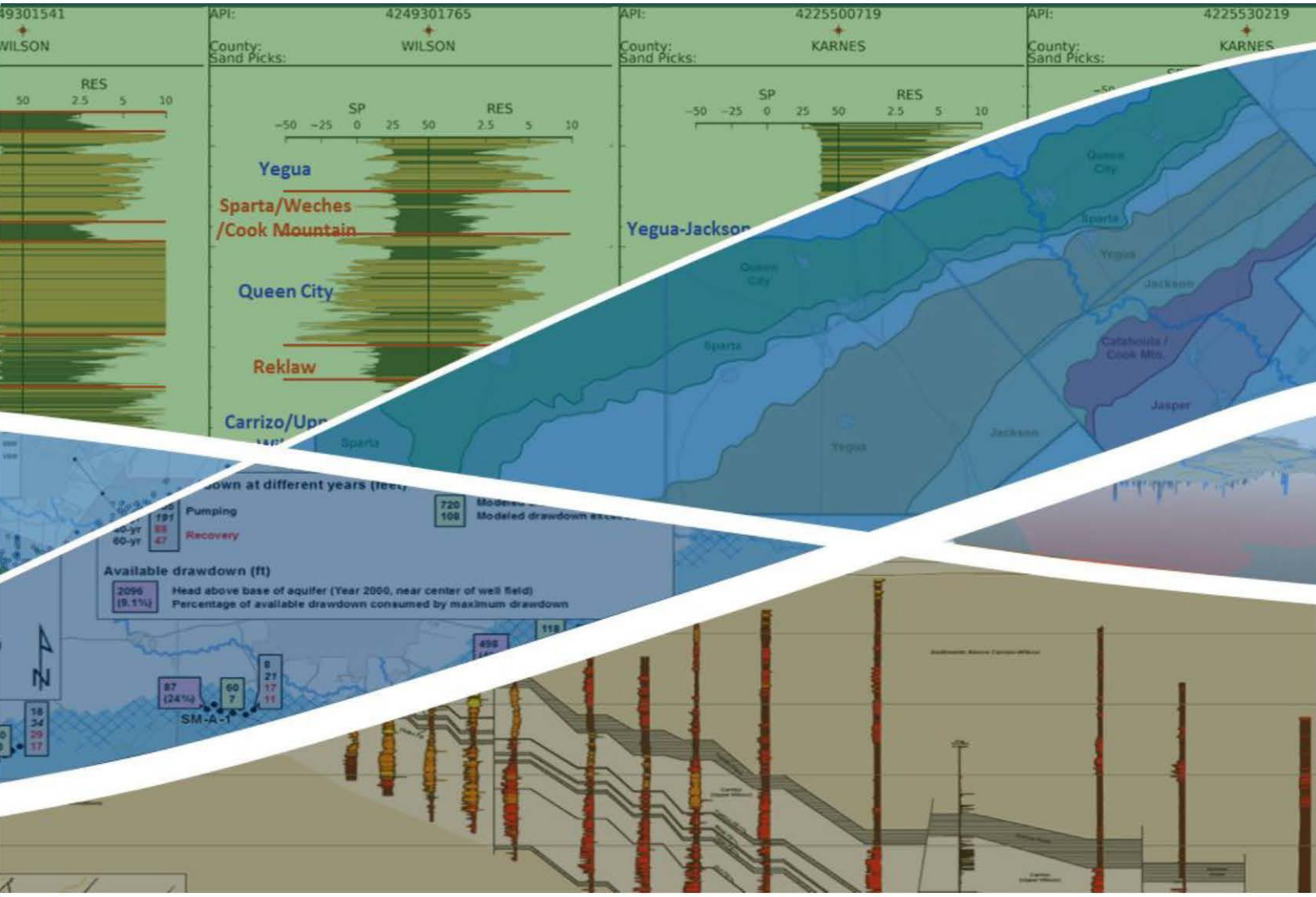

Prepared For

EUWCD

Prepared By

INTERA
GEOSCIENCE & ENGINEERING SOLUTIONS

July 2018

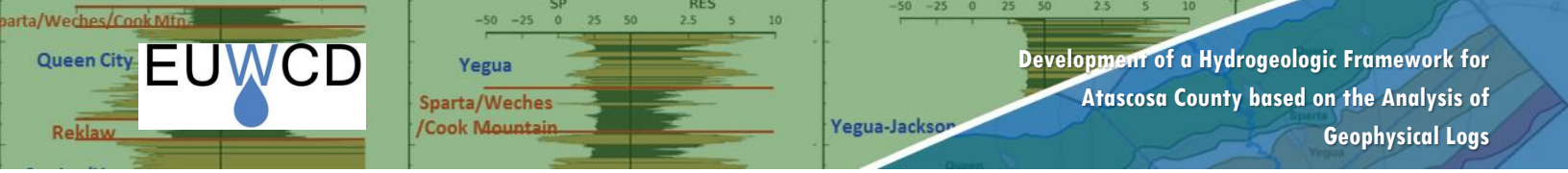

DEVELOPMENT OF HYDROGEOLOGIC FRAMEWORK FOR ATASCOSA COUNTY BASED ON THE ANALYSIS OF GEOPHYSICAL LOGS

Prepared for:

Evergreen Underground Water Conservation District
11 Wyoming Boulevard
Pleasanton, TX 78064
830.569.4186

Prepared by:

Steven Young, PE, PG, PhD
Tom Ewing, PG, PhD
Daniel Lupton, PG

July 2018

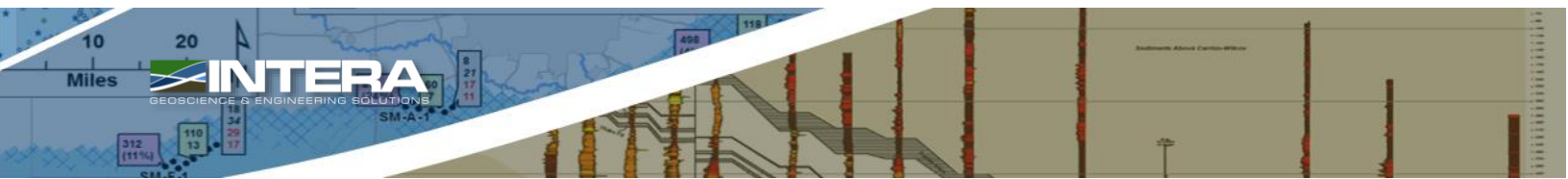

EXECUTIVE SUMMARY

The study analyzed 97 geophysical logs to create five cross-sections through Atascosa County. The cross-sections include three dip cross-sections and two strike cross-sections. The cross-sections show the stratigraphic boundaries, shale layers, and different water quality classifications of groundwater in the sand layers for the Carrizo-Wilcox, Queen City, Sparta, and Yegua-Jackson aquifers. The stratigraphic boundaries for the Carrizo-Wilcox Aquifer are based on a chronostratigraphic framework. This framework was used to map ten major transgressive shales that are key markers and boundaries for delineating the Carrizo-Wilcox Aquifer. Three of these shales are located in the Middle Wilcox and jointly act as an effective barrier to groundwater flow between the Carrizo/Upper Wilcox and Lower Wilcox aquifers. One of the shales that was mapped but is above the Carrizo-Wilcox Aquifer is the Reklaw Formation. The Reklaw Formation is typically more than 200 feet thick across most of Atascosa County, is easily traceable between logs, and serves as an effective hydrogeologic barrier to groundwater flow between the Queen City Aquifer above it and the Carrizo/Upper Wilcox Aquifer below it. In addition, the shales associated with the Cook Mountain were mapped and these shales serve to isolate the Yegua-Jackson from aquifers below it.

The resistivity/induction and the spontaneous potential curves were analyzed for the 97 logs to identify continuous sequences of sands and clays above the base of the Carrizo-Wilcox Aquifer to the top of the log. A total of 5,982, sand intervals were identified. For each of the sand interval, the total dissolved solids (TDS) concentration of the groundwater in the sand was estimated based on the resistivity value of the sand interval. The TDS concentrations calculated from the resistivity values were used to group the water quality of the groundwater into the following classifications: fresh water (TDS concentration less than 1,000 milligrams per liter [mg/L]), slightly saline (TDS concentration between 1,000 and 3,000 mg/L), moderately saline (TDS concentration between 3,000 and 10,000 mg/L), and very saline (TDS concentration above 10,000 mg/L). The Carrizo/Upper Wilcox Aquifer contains freshwater at much greater depths than any formation. In all three dip cross-section, freshwater occurs to depths approaching 4,500 feet and slightly saline groundwater occurs at depths between 4,500 and 5,000 feet.

GEOSCIENTIST AND/OR PROFESSIONAL ENGINEER SEAL(S)

Steven C. Young, P.E., P.G., Ph.D.

Dr. Steven Young was the project manager and was primarily responsible for writing the report, selecting many of the logs, checking the picks on log analysis for consistency and accuracy, and developing an approach for integrating data from several projects.

07/30/2018

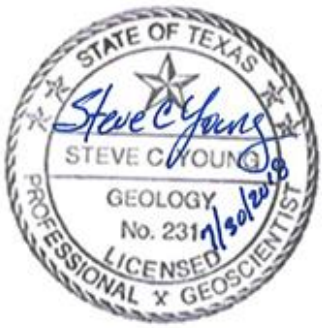

Tom Ewing , P.G., Ph.D.

Dr. Ewing was responsible for correlating the transgressive shales across the sections, picking the sand and clay intervals for the geophysical logs, and for delineating the stratigraphic boundaries that define the formations that comprise the Wilcox Aquifer.

07/30/2018

Daniel Lupton, P.G.

Daniel Lupton was responsible for creating the PETRA Project, constructing and finalizing the stratigraphic picks on the cross-sections and developing the approach for estimating the Total Dissolved Solid concentrations for individual aquifer units based on the formation water resistivity as interpreted from geophysical logs run in oil and gas wells.

07/30/2018

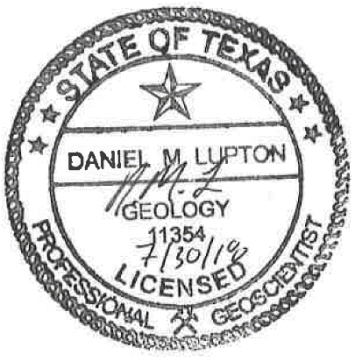

TABLE OF CONTENTS

LIST OF FIGURES

LIST OF TABLES

ACROYNMS AND ABBREVIATIONS

API	American Petroleum Institute
cm	centimeters
Cy	Clayton Shale
Du	Dull Shale
EUWCD	Evergreen Underground Water Conservation District
GAM	Groundwater Availability Model
GMA	Groundwater Management Area
Hb	Hobson Shale
INTERA	INTERA Incorporated
Kn	Kenedy Shale
mg/L	milligrams per liter
ohm-m	ohm-meters per meter
ohm^2/m	square ohm-meters per meter
Psh	Poth Shale
R1	Reklaw 1
Rn	Runge
STEER	South Texas Energy and Economic Roundtable
SP	Spontaneous potential
Td	Tilden Shale
TDS	total dissolved solids
TWDB	Texas Water Development Board
Wb	Webb Shale
Yk	Yoakum Shale

1.0 INTRODUCTION

The Evergreen Underground Water Conservation District (EUWCD) includes Atascosa, Frio, Karnes, and Wilson counties. The District manages its groundwater resources with the goal of conserving the resources while seeking to maintain the economic viability of all water resource user groups, public and private. In consideration of the economic and cultural activities occurring within the District, the District identifies and promotes best management practices of all groundwater resources within the District. In pursuit of its mission to promote best management practices, the District supports technical studies to improve the characterization and modeling of its groundwater resources.

1.1 Background Information

An objective of the study is to provide hydrogeological information helpful for improving the management of groundwater resources in the District. The components of the hydrogeological framework include stratigraphic picks that delineate the major and minor aquifers, lithologic picks that identify the location of major intervals of sands or clays, and water quality picks that map the major salinity zones in the major and minor aquifers.

This study builds on the study by Lupton and others (2017) that presents a hydrogeologic framework developed for Karnes and Wilson counties based on the analysis of geophysical logs. As Lupton and others' (2017) study did, the study for Atascosa County builds on information and data generated from the following three projects: (1) an EUWCD-funded project focused on developing a detailed stratigraphy of the Carrizo-Wilcox Aquifer underlying Wilson and Atascosa counties; (2) a Texas Water Development Board (TWDB)-funded project focused on delineating the stratigraphy and characterizing groundwater quality of the Carrizo-Wilcox Aquifer in Groundwater Management Area (GMA) 13; and, (3) a South Texas Energy and Economic Roundtable (STEER)-funded project focused on assembling and integrating hydrogeological data to support the improving aquifer characterization of the major and minor aquifers in EUWCD.

The study presents the analysis of 97 geophysical logs to delineate stratigraphy, sand and clay intervals, and the total dissolved solids (TDS) concentrations in groundwater along five vertical cross-sections in Atascosa County. **Figure 1** shows the location of the five cross-sections. Cross-sections C, D, and E, are aligned along geologic dip, and cross-sections S3 and S4 are aligned along geologic strike. For each cross-section, the location of geophysical logs are marked using black dots. **Figure 2** shows geophysical logs in **Figure 1**, along with the five vertical cross-sections provided by Lupton and others (2017) for Karnes and Wilson counties.

1.2 Report Organization

The report includes two main sections and a summary. **Section 2** provides an introduction and background information describing geophysical logs. The primary log types used as part of this study are resistivity/induction and spontaneous potential (SP). **Section 3** describes the methodology used for the log analysis and presents plots of stratigraphy, lithology, and water quality along five cross-sections. The information present in the plots is consistent with results from several previous studies, including Hargis (2015a,b; 2009) and Hamlin and others (2016). **Section 4** provides a brief summary of the findings, while **Section 5** includes a list of references.

2.0 GEOPHYSICAL LOGS

Borehole geophysics involves recording and analyzing physical and electrical property measurements made in a borehole (or a well). Geophysical measurements are made by lowering a sonde into the borehole on the end of an electric cable. The majority of the work associated with this study involves the assembling and analysis of geophysical logs to evaluate physical and electronic signatures in support of the characterization of aquifer stratigraphy, lithology, and water quality.

2.1 Types of Borehole Geophysical Logs

Because the first geophysical borehole logs were made more than seventy years ago, a number of probes have been developed to measure nearly every possible physical parameter in a borehole. The different logging tools are not named according to any particular system. Some are named on the basis of the parameter measured, others according to the principle by which the measurement is made, and still others on the basis of the geometry of the probe or the trade name. **Table 2-1** summarizes basic information on the most important and widely applied logging tools in hydrogeology.

Table 2-1 General description of types of geophysical logs

Log type	Specific log	Borehole Conditions	Information
Nuclear	Gamma-ray Gamma-gamma (density) Neutron-neutron (porosity)	Open and cased holes with or without fluid Open holes with fluid	Lithology, density, porosity, calibration of surface geophysics
Electrical	Spontaneous Potential Resistivity Focused Resistivity	Open or screened holes with fluid	Lithology, salinity of groundwater, calibration of surface geophysics, location of PVC screens
Electromagnetic	Induction Nuclear magnetic resonance	Open and PVC cased holes with or without fluid	Lithology, salinity of groundwater
Acoustical	Sonic	Open holes with fluids	Lithology (porosity)
Optical	Borehole camera Optical borehole televiewer	Borehole camera Optical borehole televiewer	Borehole camera Optical borehole televiewer
Flow	Impeller flowmeter Heat pulse flowmeter	Open and cased holes with fluid	Vertical water movement in the borehole
Fluid	Water quality	Open and cased holes with fluid	EC, temperature, pH, O_2, NO_3, Eh, total gas pressure

The three types of geophysical logs used that were analyzed as part of this the study are resistivity, induction, and SP. Each of these types of geophysical logs are described in the following subsections.

2.1.1 Resistivity Log

In conventional resistivity logging, an electric current is forced to flow between two electrodes, and the resulting electric potential (voltage) is measured between two other electrodes. Resistivities of surrounding geologic material is computed from the voltage measurement. The unit of resistivity (reciprocal of conductivity) measurement is the square ohm-meter per meter (ohm^2/m).

Dry formations will have very high resistivities because they are poor conductors of electricity. Saturation of a deposit reduces its resistivity because water is an electrical conductor. In general, saturated subsurface materials with low resistivity include silts, clays, and shales. Fresh water deposits composed of sands and gravel tend to have high resistivities. The resistivity of a formation will vary inversely with the TDS concentrations in its pore water. One of the reasons that clays tend to have low apparent resistivities is because their interstitial waters are often highly mineralized. On the other hand, sands and gravels saturated with fresh water tend to have high apparent resistivities because their surfaces are relatively inert and tend to release few minerals into solution.

Figure 3 illustrates how apparent resistivity can vary with differences in subsurface material and TDS concentration in groundwater. The difference in apparent resistivity between sandy and clayey deposits is considerably greater in fresh water than in very brackish water. In fact, in salt water, the difference in apparent resistivity between clay and sand is subtle. In situations that involve heterogeneous deposit types and vertical variations in water quality, analysis of the resistivity logs should be performed in concert with the analysis of other logs that provide independent information on either the characteristics of the deposits or the water quality.

Because the borehole fluids affect the resistivity measurement, the borehole diameters should be kept as small as possible. In a large-diameter hole or with short spacings between the electrodes, the resistivity will be heavily influenced by the drilling fluid. This is because the "zone of influence" of the electrodes may not extend very far into the formation (Driscoll, 1986). To help identify and account for the influence of the borehole fluids, several electrode spacings may be used to obtain different degrees of penetration into the surrounding geological material. The resistivity logs that were most commonly analyzed for this study consist of two electrodes downhole. When the separation of the electrodes is 16 inches or less, the configuration is called a short normal. If the two electrodes are separated by 64 inches, the configuration is called a long normal. The larger the spacing between the two downhole electrodes, the deeper the penetration of the measurement into the formation.

2.1.2 Induction Logs

Induction logs provide similar information to resistivity logs. However, the induction logging tool can be used in dry boreholes, in boreholes containing nonconducting fluids, and in polyvinyl chloride-cased boreholes, whereas resistivity tools cannot.

Instead of using electrodes to generate electric current in the subsurface, a borehole induction tool uses electric coils to create magnetic fields that in turn induce electric currents in the subsurface. The induced electrical eddy currents are proportional to the conductivity of the rock. An induction tool usually contains two coil systems with different coil spacings and thus different investigation depths. Coil systems with several transmitter and receiver coils are used to focus the field to minimize the influence of the borehole itself on the recorded signal. The investigation depth depends on the conductivity of the rock and is 60 – 350 centimeters (cm) for a dual induction log.

2.1.3 Spontaneous Potential Log

SP logs record naturally occurring electrical potentials (voltages) that occur in the borehole at different depths. The SP log primarily measures the electrochemical potential between a stationary reference at the surface and a moving electrode in the borehole.

The circuitry between the surface and the downhole electrode does not include an external source for an electric current. The electrochemical potential is generated by ions moving between the borehole fluid and the formation water. If there is no contrast in the ionic concentrations of the borehole fluid and the formation water, there is no electrochemical potential, and therefore the SP is zero. The downhole electrode usually has a lower (more negative) potential than the surface electrode. SP logs only record relative values rather than the absolute values measured by resistivity tools.

Figure 3 illustrates SP responses that can be expected in formations containing fresh water, brackish water, and salt water when the drilling fluid is composed of fresh water. As shown in Figure 3, at shallow depths where there may be little difference in the concentration of ions between the drilling fluids and the aquifer, the analysis of the SP log may be difficult because of the lack of deflections. However, at deeper depths where the formation waters are more mineralized than the drilling fluids, the leftward deflections (more negative values) in the SP logs are useful for identifying permeable strata. The analysis of an SP log begins with developing a "baseline" by connecting the potentials associated with the impermeable beds such as clays and shales as shown with the dashed line in Figure 2. Deflections to the left of this baseline are usually associated with beds of coarse-grained deposits such as sands and gravels. If no clay layers are present in the lithologic profile, the SP log may not provide much useful information.

2.2 Geophysical Logs Used for the Study

A total of 97 geophysical logs were used for this study. The logs were obtained from three sources. The primary source of logs were DVDs provided to EUWCD by Dr. Richard Hargis, who completed a multi-year study in 2015 that focused on identifying and mapping transgressive shales in the Wilcox Group. The majority of Dr. Hargis' work is summarized in two reports. Hargis (2015a) focuses on log analysis in Atascosa County, whereas Hargis (2015b) focuses on log analysis in Wilson County. Additional logs were obtained by the Geophysical Log Facility at the Bureau of Economic Geology in Austin, Texas, the Subsurface Library in Austin Texas, and the Balcones Energy Log Library in San Antonio, Texas.

Table 2-2 lists the number of logs associated with the five cross-sections. For each of the cross-sections, Table 2-2 also lists the number of logs that were also used as part of cross-sections associated with two related hydrogeologic studies of the Wilcox Aquifer. Forty-nine of the logs overlap with the logs used by Hargis (2015a,b; 1986). Three of the logs were used by a TWDB-funded study to characterize the brackish groundwater associated with the Wilcox Aquifer in GMA 13.

Table 2-2 Number of logs associated with each cross-section

Cross-Section	Number of Geophysical Logs		
	Total	Used by Hargis (2015a,b; 1986)	Used by Hamlin and others (2016)
Dip C-C'	30	6	2
Dip D-D'	24	16	0
Dip E-E''	21	14	1
Strike S3-S3'	17	15	0
Strike S4-S4'	12	1	0

3.0 CONSTRUCTION OF CROSS-SECTIONS

The cross-sections were developed using software called PETRA (IHS, 2009). PETRA is a commercial software widely used in the oil and gas industry to manage and analyze geophysical logs. All the logs were brought into PETRA as TIFF files. TIFF files are images that are created by scanning a paper copy of the geophysical logs. Prior to analyzing the TIFF files, the files were "depth registered" to facilitate the process of creating the five cross-sections. The process of depth registering involves the correcting of any distortion in the image so that accurate elevation picks can be made by marking the image.

3.1 Stratigraphy

The construction of the three dip sections began with stratigraphic picks provided by Hargis (2015a,b) for 49 logs in Atascosa County. EUWCD commissioned Richard N. Hargis in November of 2008 to perform a stratigraphic analysis of the Wilcox Group for their District. Mr. Hargis' qualifications for Carrizo and Wilcox stratigraphic and structural interpretation are exemplary. He has been recognized by numerous geological societies for his in-depth understanding of the Carrizo and Wilcox stratigraphic intervals. Hargis (1985, 1986) provides the general approach for the defining the stratigraphic of the Wilcox Group is south Texas. In 2009, Hargis (2009) identified the ten major transgressive shales shown in **Figure 4** as the key markers and boundaries for delineating the Wilcox Formation. The names and abbreviation of these ten shales are the Reklaw 1 (R1), Hobson (Hb), Runge (Rn), Kenedy (Kn), Clayton (Cy), Dull (Du), Yoakum (Yk), Webb (Wb), Tilden (Td) and Poth (Psh) Shales. The Hobson and Dull Shales are present only along the southeast fringe of the study area. The shales are the most extensive marine transgressions in the Wilcox in the northern portion of South Texas for a specific time horizon. These shales form the natural boundaries and likely serve as an aquitard over the area covered by the shale. **Figures 5** and **6** show the up-dip areal extent of the shales.

The 49 logs from Hargis (2015a,b) that served as the kernel for the study are associated with the dip cross-sections C, D, and E constructed by Hargis (2015a,b) for Atascosa County. The remaining 48 logs were assembled by INTERA Incorporated (INTERA) and Dr. Tom Ewing . The stratigraphic picks made for study were primarily performed by Dr. Ewing. During the generation of the cross-sectional that shown water quality and stratigraphic picks, INTERA made several minor adjustments in the picks to improve the lateral continuity of the shales and formations and consistency with water quality picks.

Figures 6 through **10** show the five cross-sections with stratigraphy. The vertical axis is scaled to represent elevation reference to sea level. At the top of each geophysical log is the American Petroleum Institute (API) number for the log or the identification number that Dr. Hargis assigned to the log. In each of the cross-sections, the shale units are colored gray as they correlate between logs. Most of these shales are continuous over their extent except in the vicinity of faults, whose locations are approximated by slanted lines across which there are offsets in the elevation of the shales.

3.2 Lithology

Dr. Ewing performed most of the lithology picks in PETRA. The lithology picks consisted of marking the top elevation of sands and clays sequences based on his evaluation of both the shallow resistivity, deep resistivity, and the SP curves. A total of 5,982 sand intervals were identified on 97 logs. The digitized versions of the geophysical logs are shown in Figures 6 through 10. On the right-hand side of each log are plotted values from

either a resistivity or induction log. On the left-hand side of the of each log are plotted values from the SP curve. The distance between the logs is colored to represent either sand or clay. Clay units are colored brown and sand units are color-coded based on the estimated concentration of the TDS concentration of groundwater in the sand.

3.3 Total Dissolved Solids Concentrations

For each of the sand intervals on the geophysical logs, the TDS concentrations of the groundwater were estimated based on the resistivity value for the sand intervals. The TDS concentrations calculated from the resistivity values were used to classify the water quality of the groundwater based on the classification scheme developed by Winslow and Kister (1956) and shown in **Table 3-1**. In Figures 6 through 10, the sand intervals are color-coded based on the four water classifications described in Table 3-1.

Table 3-1 Groundwater classification based on the criteria established by Winslow and Kister (1956)

Water Classification Description	TDS Range
Fresh	Less than 1,000 mg/L
Slightly Saline	1,000 to 3,000 mg/L
Moderately Saline	3,000 to 10,000 mg/L
Very Saline	10,000 to 35,000 mg/L

Note: TDS=total dissolved solids; mg/L=milligrams per liter

The TDS concentrations for the sand intervals was estimated using an approach called the Mean R_o Method, which involves calculating TDS from resistivity measurements on a geophysical log. Among the studies that have used the Mean R_o Method in either the Gulf Coast Aquifer System or the Carrizo-Wilcox Aquifer are: Fogg and Blanchard (1986), Hamlin and others (1988), Collier (1993), Estepp (1998), Hamlin and Luciana de la Rocha (2015), Ayers and Lewis (1985), Fogg (1980), Fogg and Kreitler (1982), Meyer (2012), Hamlin and others (2016), and Young and others (2016). For this study, the TDS concentrations was calculated using the Mean R_o Method using the deep resistivity (long normal or deep induction).

The development of the Mean R_o Method typically requires plotting TDS concentration measured in a water well against the resistivity (R_o) of the sands intersected by the well. Often, the geophysical log is from a borehole that was drilled near the well. **Figure 11** is a Ro-TDS graph developed by Hamlin and others (2016) for groundwater in the Carrizo/Upper Wilcox Aquifer in GMA 13. **Figure 12** is a R_o-TDS graph developed by Young and others (2016) for a groundwater in the Chicot Aquifer in the Texas Gulf Coast Aquifer System. The graph shows an inverse relationship between TDS concentration and formation resistivity. However, the relationship between TDS concentration and resistivity is substantially different for the two aquifer systems. The different relationship developed for the two aquifer systems is caused by a wide range of factors, including different sand and clay mineralogies, different depositional settings, different porosities, different groundwater chemistries, and different temperatures. These differences underscore the importance of obtaining site-specific data for developing the Mean R_o Method for an aquifer.

In both Figures 11 and 12, there is scatter of data points about the best fit line used to represent the relationship between resistivity and TDS concentration. The scatter in the data exists partly because the R_o Method does not explicitly account for differences in chemical composition of the TDS concentration, effects of mud filtrate,

resolution of the logging tool, variations in the sands, and the possible inclusion of clays in the sand layer. Despite the scatter, the standard practice is to use the relationship expressed by the straight lines in Figures 11 and 12 to estimate TDS concentrations from resistivity without providing a confidence limit that would indicate a level of uncertainty with the estimate. For example, using the relationship expressed by the line in Figure 11, a resistivity of 100 ohm-meters per meter (ohm-m) and of 10 ohm-m represent TDS concentrations of 200 milligrams per liter (mg/L) and 4,000 mg/L, respectively.

For this study, the resistivity values used to assign the TDS concentrations that are used to classify groundwater based on water quality criteria are provided in **Table 3-2**. These resistivity values were obtained from three groundwater studies that included parts or all of EUWCD. Data analysis results from Hamlin and others (2016) were used to evaluate the water quality of the Carrizo and Wilcox intervals. Data analysis results from Wise (2014) were used to evaluate the water quality of the Queen City and Sparta intervals and data analysis results from Young and others (2016) were used to evaluate the water quality in the Yegua-Jackson units. Table 3-2 is a summary of the resistivity values used from these three references to create values of resistivity for calculating TDS concentrations of 1,000, 3,000, and 10,000 mg/L for the different formations and aquifers in Figures 6 through 10.

Table 3-2 Summary of resistivity cutoff values for the various water quality categories

Aquifer	TDS (mg/L)	R_o (ohm-m)	Source
Yegua-Jackson	1,000	12.3	Young and others (2016) Table 13-24 (Jasper)
Yegua-Jackson	3,000	4.5	Young and others (2016) Table 13-24 (Jasper)
Yegua-Jackson	10,000	2.7	Young and others (2016) Table 13-25 (30% Porosity Calc)
QCSP	1,000	31.1	From BRACS database for TN 14-01 (Wise, 2014)*
QCSP	3,000	11.5	From BRACS database for TN 14-01 (Wise, 2014)*
QCSP	10,000	3.9	From BRACS database for TN 14-01 (Wise, 2014)*
Carrizo	1,000	25.0	Hamlin and others (2016) Table 4-2 (NE)
Carrizo	3,000	10.0	Hamlin and others (2016) Table 4-2 (NE)
Carrizo	10,000	4.0	Hamlin and others (2016) Table 4-2 (NE)
Wilcox	1,000	33.0	Hamlin and others (2016) Table 4-3
Wilcox	3,000	16.0	Hamlin and others (2016) Table 4-4
Wilcox	10,000	11.0	Hamlin and others (2016) Table 4-5

* Data related to the relationship between formation resistivity and TDS was not available within the Wise (2014) report and was therefore acquired from the BRACS database.

Several of the R_o cutoff values in Table 3-2 are not based upon a plot of measured TDS concentration versus resistivity. In these cases, there was insufficient data to create a relationship between TDS concentrations and resistivity at the concentration value of interest, so the R_o value was calculated using the R_{wa} Minimum Method.

The development of the R_{wa} Minimum Method is beyond the scope of this study but the general formulation of the method is relevant to the study so a general overview of the method is provided. The R_{wa} Minimum method uses the Archie (1942) equation to estimate TDS concentration. For the situation where the aquifer is saturated with water, the Archie Equation can be written as:

$$R_{we} = \Phi^m \times R_o \quad \text{(Equation 3-1)}$$

where

R_{we} = resistivity of water equivalent (ohm-meters)
Φ = porosity
m = the cementation exponent
R_o = the resistivity of a 100 percent water saturated formation (ohm-meters)
F = formation factor = Φ^m

In Equation 3-1, the cementation exponent is a function of the consolidation of the formation. Estepp (1998, 2010) provide guidelines for estimating the value of *m* for an aquifer. After Equation 3-1 has been applied to calculate the value of $R_{we,}$ Equation 3-2 is then used to calculate a value of C_w. Equation 3-3 is then used to calculate the TDS of the groundwater based on the value C_w. Readers interested in the details associated with developing and applying the R_{wa} Minimum Method are referred to Young and others (2016), Lupton and others (2016), and Meyer and others (2014).

$$C_w = 10{,}000 / R_{we} \quad \text{(Equation 3-2)}$$

$$TDS = ct * C_w \quad \text{(Equation 3-3)}$$

where

C_w = specific conductance (umhos/cm at 77 degrees Fahrenheit)
ct = specific conductivity-total dissolved solids concentration conversion factor
TDS = total dissolved solids concentrations (milligrams per liter)

3.4 Discussion of Cross-Sections

The five cross-sections shown in Figures 7 through 11 are separated into three dip sections (C, D and E) and two strike sections (S3 and S4). Across most of the area covered by the logs, the Sparta Aquifer is generally sand-poor and is sandwiched between two clay rich formations, the Weches and the Cook Mountain formations. From a practical perspective, these three formations have been combined into a single layer based on high frequency of shales indicated in the geophysical logs. The single layer named Cook Mountain/Sparta/Weches represents a shaly interval that prevents vertical groundwater flow. As such, the layer is colored gray along with the ten shale units identified by Hargis (2009).

Our analysis of the five cross-sections supports a simple but useful conceptual model of the groundwater flow system. The key points associated with the schema are as follows:

- There are four primary flow systems that are separated from each other by formations that are shale rich. These primary flow systems are the Yegua-Jackson, the Queen City Aquifer, the Carrizo and Upper Wilcox Aquifer, and the Lower Wilcox Aquifer.
- The two major shaly formations that restrict vertical groundwater flow are the Reklaw Formation and the Cook Mountain/Sparta/Weches Formation. Across most of the study area, there is more than 200 feet of shales associated with either formation.
- The Reklaw Formation is a thick shale formation that is easily traceable between logs and it serves as an effective hydrogeologic barrier to groundwater flow that hydraulically isolates the Queen City Aquifer above it from the Carrizo/Upper Wilcox Aquifer below it.
- The Cook Mountain/Sparta/Weches formation hydraulically isolates the Yegua-Jackson Aquifer above it from the Queen City Aquifer below it.

- Where they are present the combination of the Tilden, Webb, and Yoakum Shales represent an effective barrier to groundwater flow between the Carrizo/Upper Wilcox Aquifer and the Lower Wilcox Aquifer. All three of these shales become thinner and less continuous toward the up dip portion of each dip section. These formations are most prevalent in Dip Section E and least prevalent in Dip Section C.
- The Poth Shale is a good boundary marker for the base of the Wilcox Aquifer. Immediately below the Poth Shale the geophysical logs suggest that the deposits are shale rich for hundreds of feet.
- The Carrizo/Upper Wilcox Aquifer contains freshwater at much greater depths than any formation. In Cross-Section E, freshwater occurs to depths approaching 4,300 feet and slightly saline groundwater occurs at depths near 5,000 feet. In Cross-Section D, freshwater occurs to depths approaching 4,400 feet and slightly saline groundwater occurs at depths near 4,900 feet. In Cross-Section C, freshwater occurs to depths approaching 3,700 feet and slightly saline groundwater occurs at depths near 4,300 feet.
- For the three Dip Sections C, D, and E, the cross-sections show a significant water quality change across the Middle Wilcox Formation where the Tilden Shale is present. At these much of this area, the Middle Wilcox is separating fresh water in the Carrizo Aquifer from Moderately saline water in the Lower Wilcox Formation.

4.0 SUMMARY

The study analyzed 97 geophysical logs to create five cross-sections through Atascosa County. The cross-sections include three dip cross-sections and two strike cross-sections. The cross-sections show the stratigraphic boundaries, shale layers, and different water quality classifications of groundwater in the sand layers for the Carrizo-Wilcox, Queen City Aquifer, and Yegua-Jackson aquifers. The stratigraphic boundaries for the Carrizo-Wilcox Aquifer are based on a chronostratigraphic framework based on the work of Hargis (1985, 1986, 2009, 2015a,b) and Hamlin (1988). The keystone to the mapping the stratigraphy of the Carrizo-Wilcox aquifer is the identification and mapping of ten major transgressive shales that are significant key markers and boundaries for delineating the Carrizo-Wilcox Aquifer. These ten shales are the Reklaw, Hobson, Runge, Kenedy, Clayton, Dull, Yoakum, Webb, Tilden and Poth shales. The stratigraphic boundaries between the major and minor aquifers that are younger than the Carrizo-Aquifer are based on information from previous publications.

The resistivity/induction and the SP curves for the 97 logs were analyzed in PETRA to identify a continuous sequence of sands and clays for each log above the base of the Carrizo-Wilcox Aquifer. A total of 5,982 sand intervals were identified. The lithologic analysis shows that two shaly formations that significantly restrict vertical groundwater flow at the regional scale are the Reklaw and the Cook Mountain/Sparta/Weches formations. The Reklaw formation is typically more than 200 feet thick across most of Atascosa County, is easily traceable between logs, and serves as an effective hydrogeologic barrier to groundwater flow between the Queen City Aquifer above it and the Carrizo/Upper Wilcox Aquifer below it. In addition, the shales associated with the Cook Mountain Formation were mapped, and these shales isolate the Yegua-Jackson from aquifers below it. The shales identified by Hargis (2009) that exist within the Carrizo-Wilcox Aquifer shown good continuity between the logs and can be mapped across fault offsets. The combination of the Tilden, Webb, and Yoakum shales in the Middle Wilcox represents an effective barrier to groundwater flow between the Carrizo/Upper Wilcox and the Lower Wilcox aquifers. All three of these shales become thinner and less continuous toward the up dip portion of each dip section. These formations are most prevalent in Dip Section E and least prevalent in Dip Section C.

For each of the sand intervals identified on the geophysical logs, the TDS concentration of the groundwater was estimated based on the resistivity of the sand interval. The TDS concentrations calculated from the resistivity values was used to classify the water quality of the groundwater into the following classifications: fresh water (TDS concentration less than 1,000 mg/L), slightly saline (TDS concentration between 1,000 and 3,000 mg/L), moderately saline (TDS concentration between 3,000 and 10,000 mg/L), and very saline (TDS concentration above 10,000 mg/L). The TDS concentrations for the sand intervals was estimated using an approach called the Mean R_o Method, which involves calculating TDS from resistivity measurements on a geophysical log. The Mean R_o Method that has been applied in numerous studies in the Carrizo-Wilcox and Yegua-Jackson aquifers. For this study, the resistivity values used to assign the TDS concentrations are aquifer-dependent and are based on previous studies published by the TWDB.

The Carrizo/Upper Wilcox Aquifer contains freshwater at much greater depths than any formation. In all three dip cross-sections, freshwater occurs to depths approaching 4,000 feet and slightly saline groundwater occurs at depths between 4,500 and 5,000 feet.

5.0 REFERENCES

Archie, G.E. 1942. The electrical resistivity log as an aid in determining some reservoir characteristics: Petroleum Transactions of AIME 146: 54–62.

Ayers, W.B. and A.H. Lewis. 1985. Systems and Deep-Basin Lignite: The University of Texas at Austin, Bureau of Economic Geology.

Collier, H. 1993. Borehole geophysical techniques for determining the water quality and reservoir parameters of fresh and saline water aquifers in Texas: Texas Water Development Board, Report 343, vol. I&II.

Driscoll, F.G. 1986. Groundwater and Wells: St. Paul, MN, Johnson Filtration Systems, Inc., 1079 p.

Estepp, J. 1998. Evaluation of ground-water quality using geophysical logs: Texas Natural Resource Conservation Commission, unpublished Report, 516 p.

Estepp, J.D. 2010. Determining groundwater quality using geophysical logs: Texas Commission on Environmental Quality, unpublished report, 85 p.

Fogg, G.E. 1980. Geochemistry of ground water in the Wilcox aquifer, *in* Kreitler, C.W., Agagu, O.K., Basciano, J.M., Collins, E.W., Dix, O., Dutton, S.P., Fogg, G.E., Giles, A.B., Guevara, E.H., Harris, D.W., Hobday, D.K., McGowen, M.K., Pass, D. and Wood, D.H., 1979, Geology and Geohydrology of the East Texas Basin A Report on the Progress of Nuclear Waste Isolation Feasibility Studies: The University of Texas at Austin, Bureau of Economic Geology (1979), Geologic Circular No. 80-12, p. 73-78.

Fogg, G.E., and P.E. Blanchard. 1986. Empirical relations between Wilcox groundwater quality and electric log resistivity, Sabine Uplift area, *in* Kaiser, W.R. ed., Geology and Groundwater hydrology of deep-basin lignite in the Wilcox Group of East Texas: The University of Texas at Austin, Bureau of Economic Geology, Special Report No. 10, p. 115-118.

Fogg, G.E. and C.W. Kreitler. 1982. Ground-water hydraulics and hydrochemical facies in eocene aquifers of the East Texas Basin. The University of Texas at Austin, Bureau of Economic Geology, Report of Investigations No. 127, 75 p

Hamlin, H.S. 1988. Depositional and ground-water flow systems of the Carrizo-Upper Wilcox, South Texas: The University of Texas at Austin, Bureau of Economic Geology, Report of Investigations No. 175

Hamlin, H. and L. de la Rocha. 2015, Using electric logs to estimate groundwater salinity and map brackish groundwater resources in the Carrizo-Wilcox Aquifer in South Texas: GCAGS Journal v.4 (2015), p. 109-131.

Hamlin, H.S., D.A. Smith, and M.S. Akhter. 1988. Hydrogeology of Barbers Hill salt dome, Texas coastal plain: The University of Texas at Austin, Bureau of Economic Geology, Report of Investigations No. 176, 41 p.

Hamlin, S., B.R. Scanlon, R. Reedy, S.C. Young, and M. Jigmond. 2016. Fresh, Brackish, and Saline Groundwater in the Carrizo-Wilcox Aquifer in Groundwater Management Area 13 -- Location, Quantification, Producibility, and Impacts

Hargis, R. N. 1985. Proposed lithostratigraphic classification of the Wilcox Group of South Texas: Gulf Coast Association of Geological Societies Transactions, v. 35, p. 107–159.

Hargis, R. N. 1986. Proposed Stratigraphic Classification of the Wilcox of South Texas: Contributions to the Geology of South Texas, 1986, South Texas Geological Society, p.135-159.

Hargis, R. N. 2009. Major Transgressive Shales of the Wilcox, Northern Portion of South Texas, South Texas Geological Society Bulletin, April 2009, p. 19-47.

Hargis, R. N. 2015a. Report on Study of Wilcox Group Northern Atascosa County and Adjacent Areas of Bexar and Wilson Counties, prepared for the Evergreen Underwater Conservation District, Pleasanton, TX

Hargis, R. N. 2015b. Report on Study of Wilcox Group Wilson County Study Area and Adjacent Areas of Bexar and Wilson Counties, prepared for the Evergreen Underwater Conservation District, Pleasanton, TX

IHS. 2009. User's Manual for PETRA. Information Handling Services, Houston, TX.

Kelley, V.A., N.E. Deeds, D.G. Fryar, and J-P Nicot. 2004. Groundwater Availability Models for the Queen City and Sparta Aquifers: prepared for the Texas Water Development Board.

Lupton, D., V. Kelley, D. Powers, and C. Torres-Verdin. 2016. Identification of Potential Brackish Groundwater Production Areas – Rustler Aquifer. Prepared for the Texas Water Development Board, Austin, TX

Lupton, D., Young, S.C., and Hamlin, S., 2017. Development of Hydrogeologic Framework for Karnes and Wilson Counties Based on the Analysis of Geophysical Logs. Prepared for the Evergreen Underground Water Conservation District, Pleasanton, TX.

Meyer, J.E. 2012. Geologic characterization of and data collection in the Corpus Christi Aquifer Storage and Recovery Conservation District and surrounding counties: Texas Water Development Board, Austin, TX, Open File Report 12-01.

Meyer, J.E., A. Croskrey, M.R. Wise, and S. Kalaswad. 2014. Brackish Groundwater in the Gulf Coast Aquifer, Lower Rio Grande Valley, Texas: Texas Water Development Board Report 383, 107 p.

Winslow, A.G., and L.R. Kister. 1956. Saline-water resources of Texas: U.S. Geological Survey Water-Supply Paper 1365, 105 p.

Wise, M, R. 2014. Queen City and Sparta Aquifers, Atascosa and McMullen Counties, Texas: Structure and Brackish Groundwater. Technical note 14-01. Texas Water Development Board, Austin TX

Young, S. C., M. Jigmond, N. Deeds, J. Blainey, T.E. Ewing, and D. Banerji. 2016. Final Report Identification of Potential Brackish Groundwater Production Areas – Gulf Coast Aquifer System., prepared for the Texas Water Development Board, Austin, TX.

FIGURES

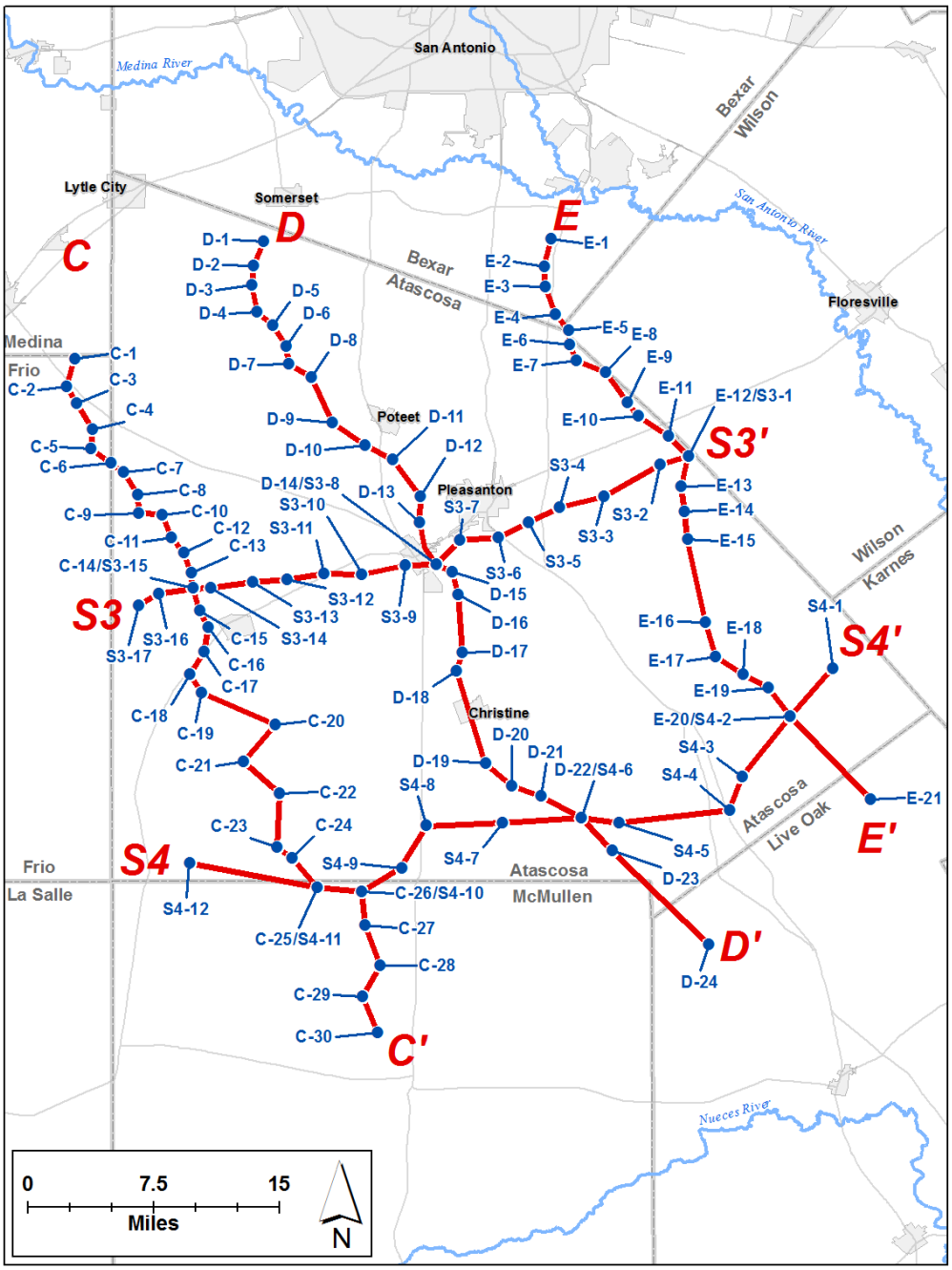

Figure 1 Location of 95 geophysical logs used to construct Dip Sections C, D, and E and Strike Sections S3 and S4 in Wilson and Karnes counties

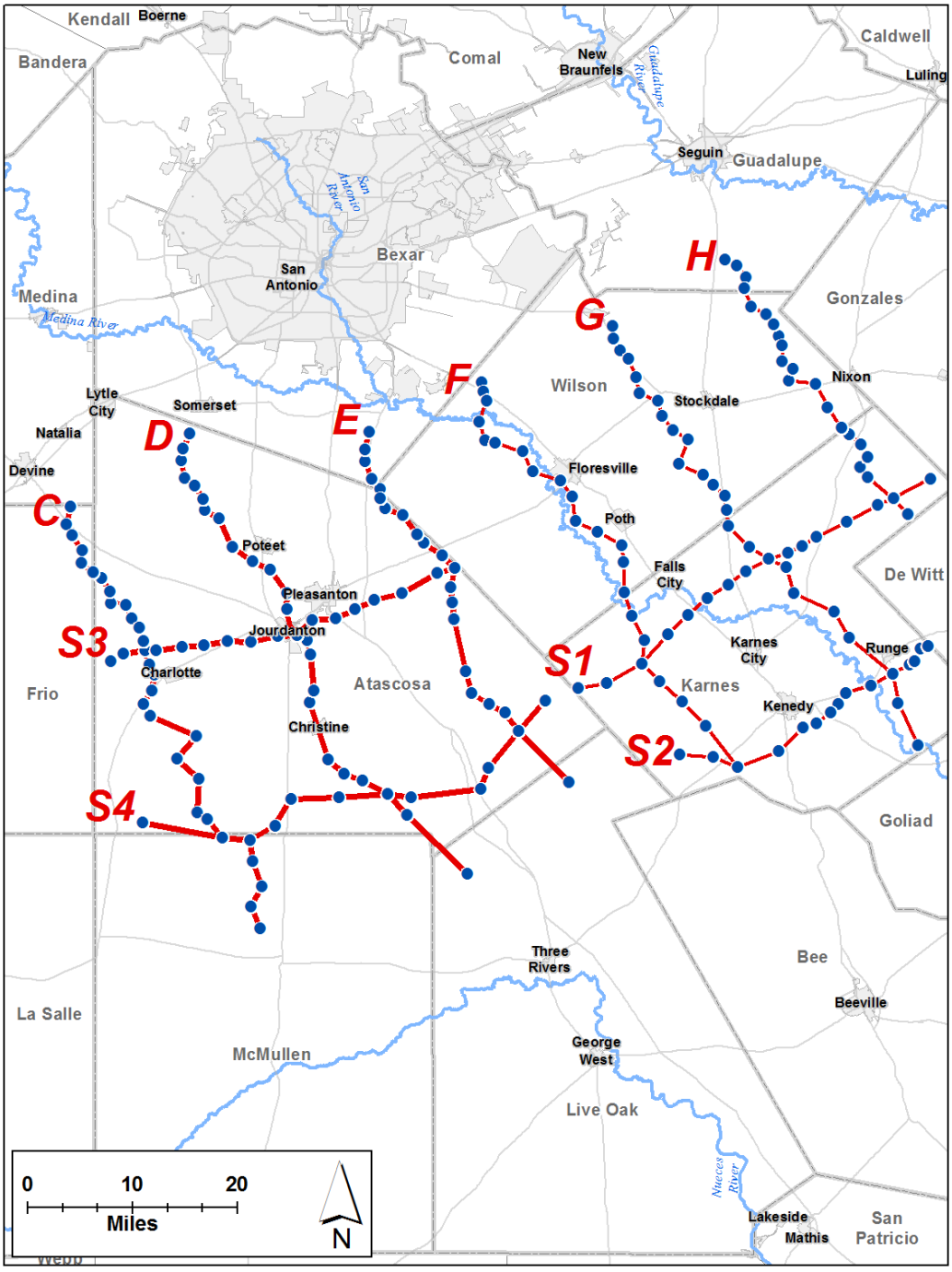

Figure 2 Location of 95 geophysical logs used to construct Dip Sections C, D, and E and Strike Sections S3 and S4 in Wilson and Karnes counties

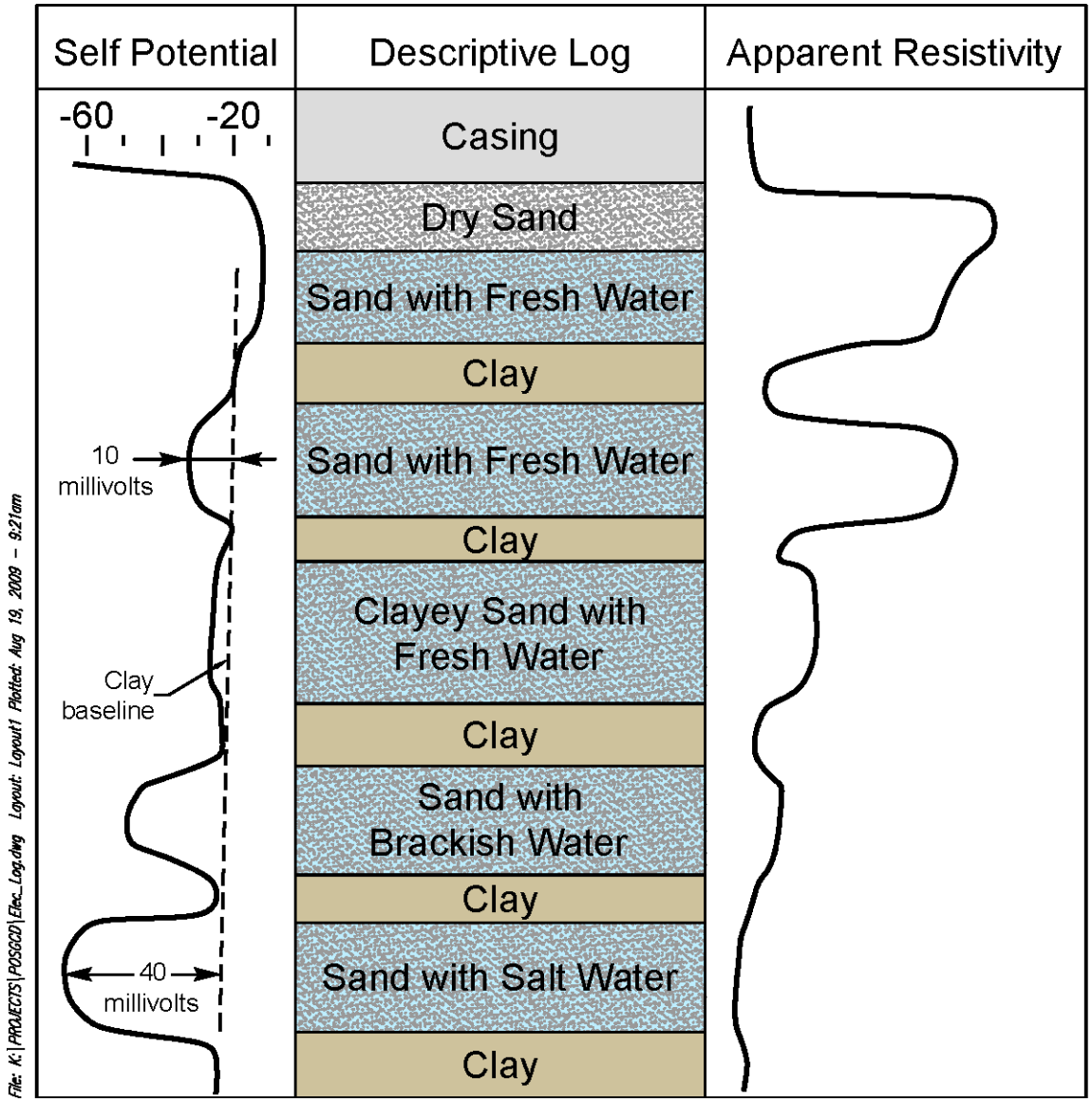

Figure 3 Idealized SP and resistivity curve showing the responses corresponding to alternating sand and clay strata that are saturated with groundwater which increases significantly in TDS concentrations with depth. Modified from Driscoll (1986, p. 189).

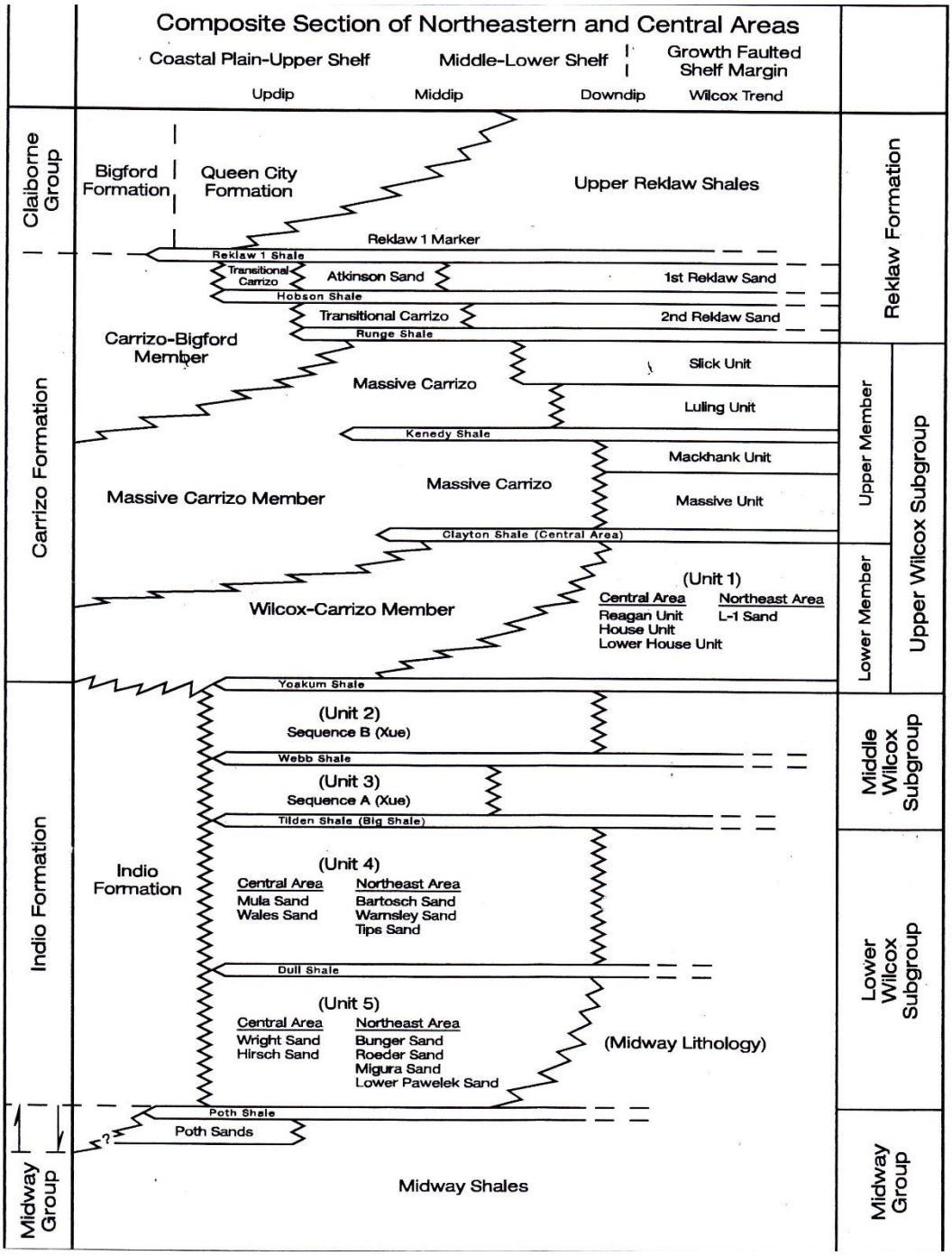

Figure 4 Classification of Wilcox Group including the stratigraphic position of ten major transgressive shales used by Hargis (2009). (Figure taken from Hargis [2015a].)

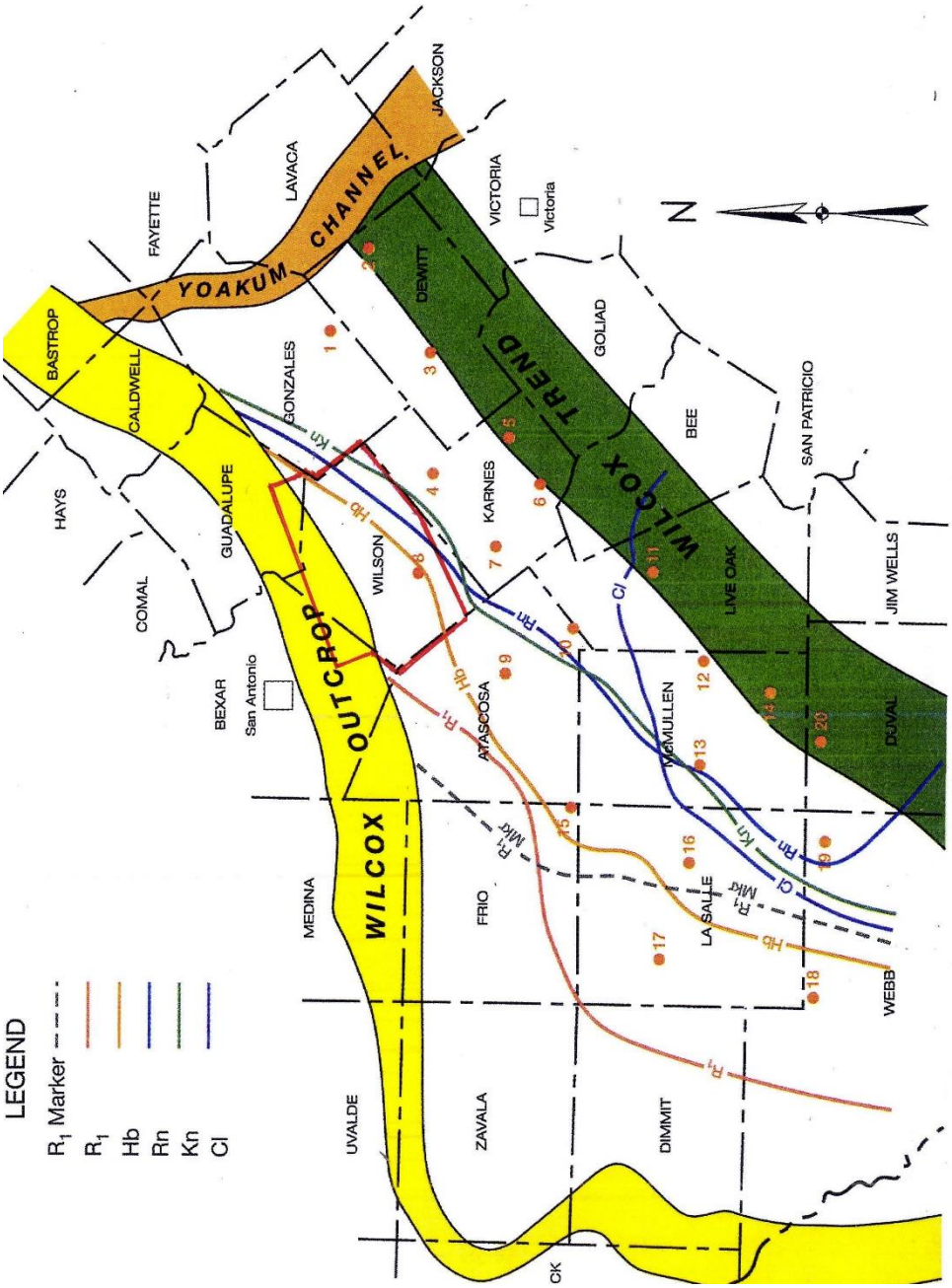

Figure 5 Approximate regional limits of Reklaw Shale (R1), Hobson Shale (Hb), Runge Shale (Rn), and Kenedy Shale (Kn) in the vicinity of Evergreen Underground Water Conservation District. (Figure copied from Hargis [2015b].)

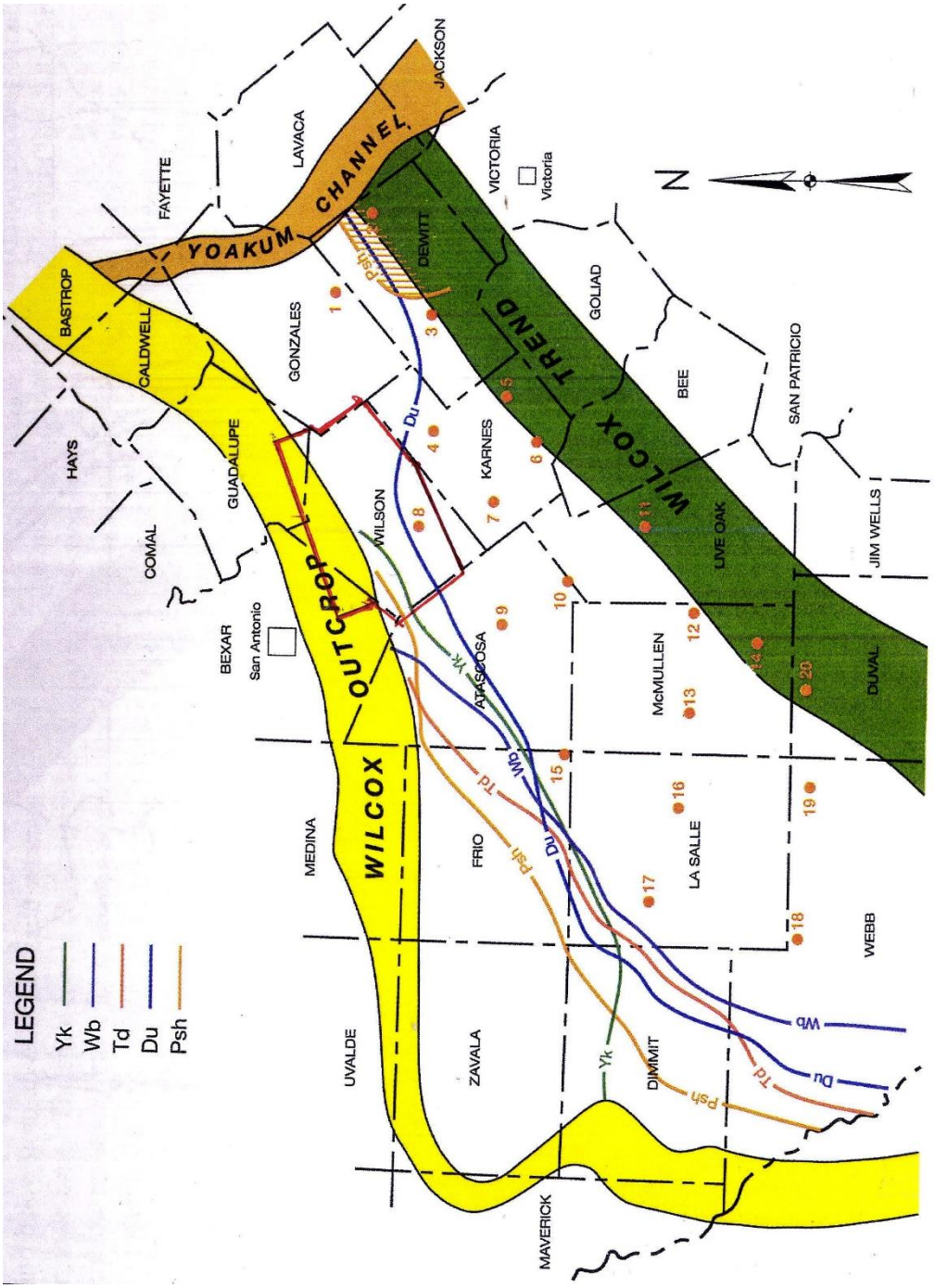

Figure 6 Approximate regional limits of Yoakum Shale (Yk), Webb Shale (Wb), Tilden Shale (Td), Dull Shale (Du) and Poth Shale (Psh) in the vicinity of Evergreen Underground Water Conservation District. (Figure copied from Hargis [2015b].)

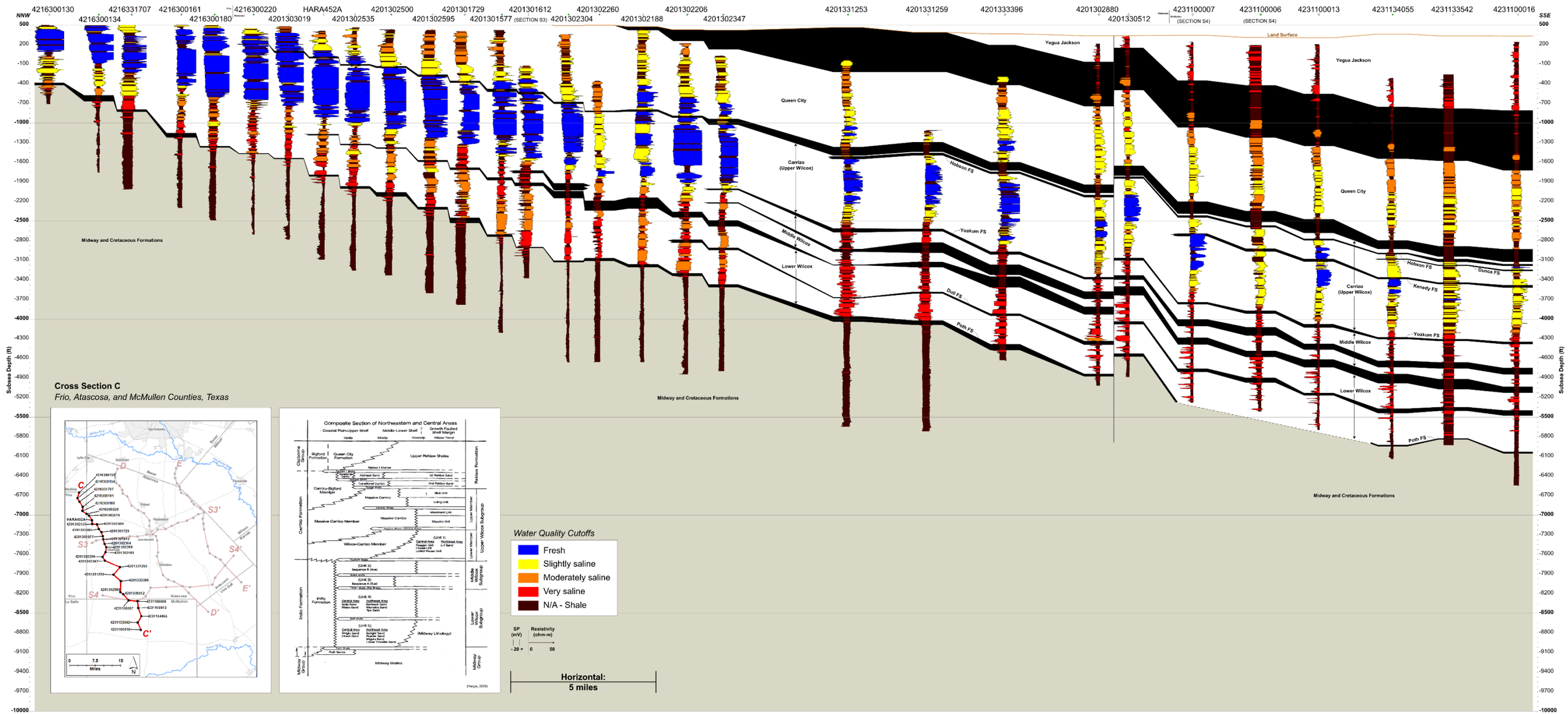

Figure 7 Dip cross-section C showing stratigraphy, shale locations, sand intervals, and water quality classifications at 30 log locations

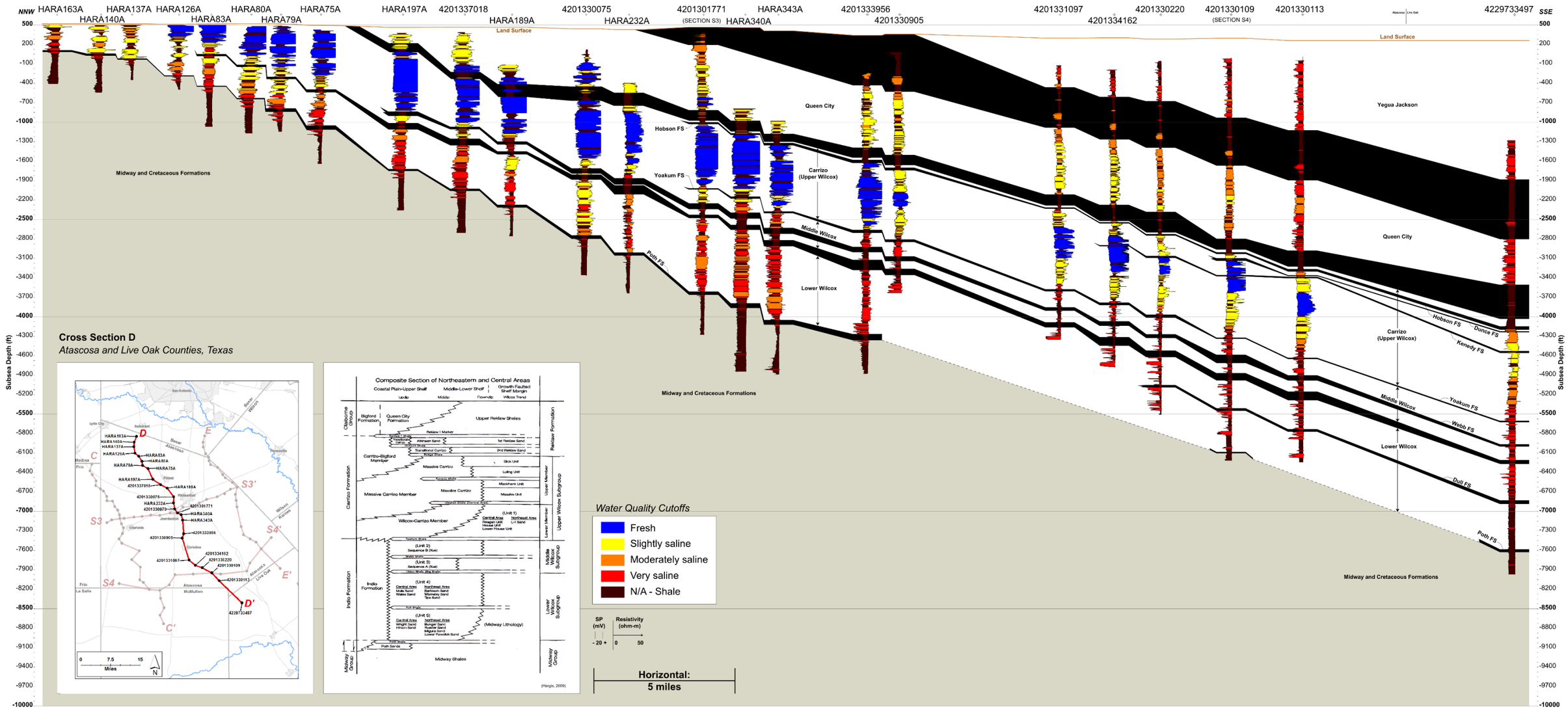

Figure 8 Dip cross-section D showing stratigraphy, shale locations, sand intervals, and water quality classifications at 24 log locations

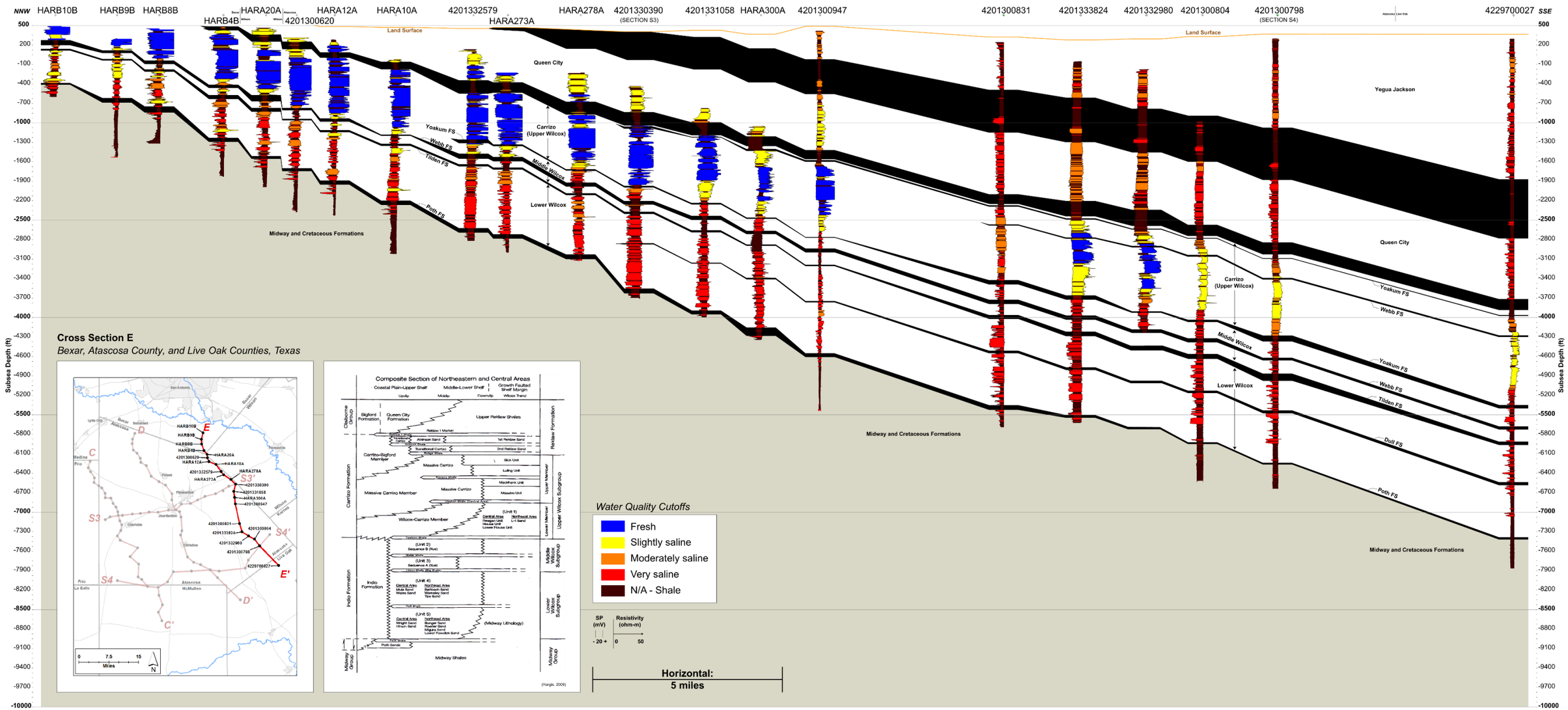

Figure 9 Dip cross-section E showing stratigraphy, shale locations, sand intervals, and water quality classifications at 21 log locations

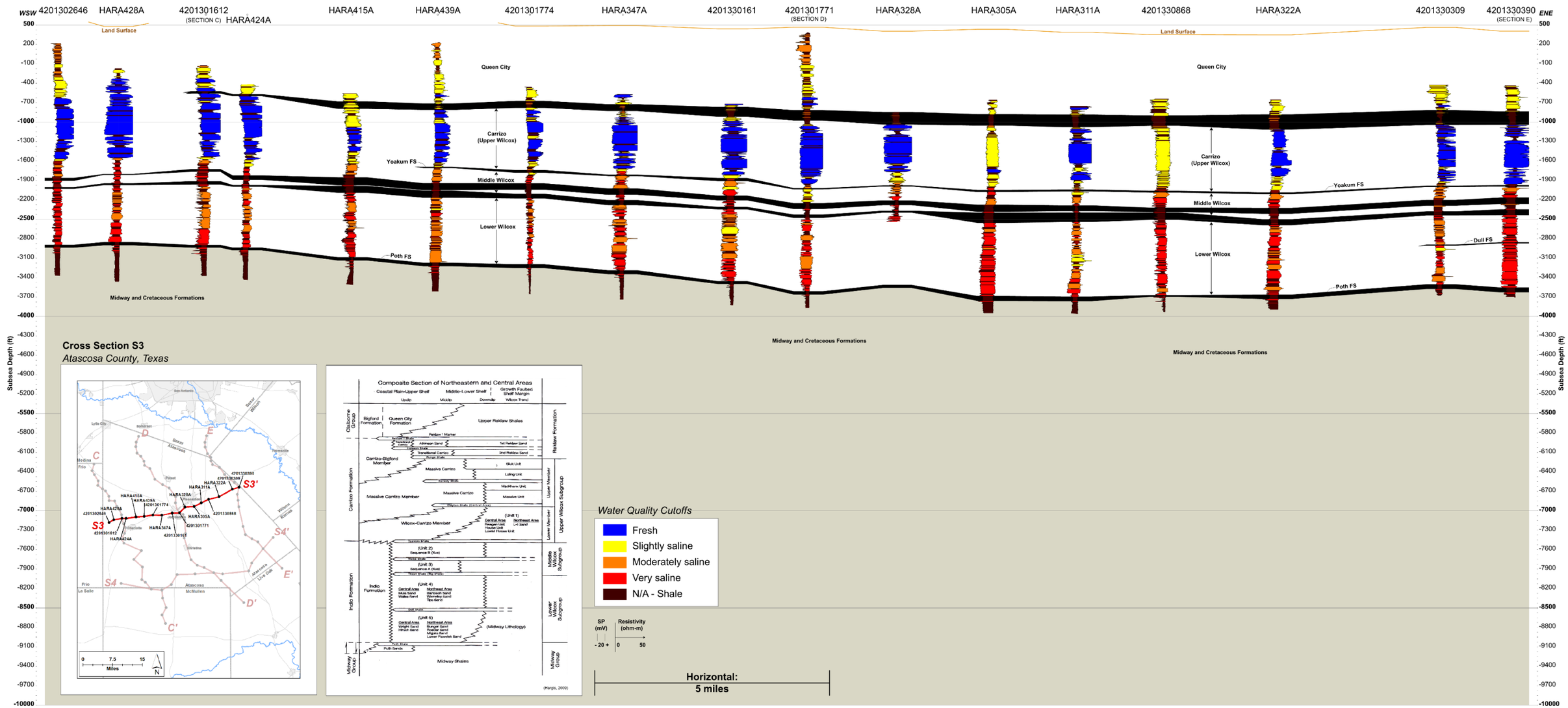

Figure 10 Strike cross-section S3 showing stratigraphy, shale locations, sand intervals, and water quality classifications at 17 log locations

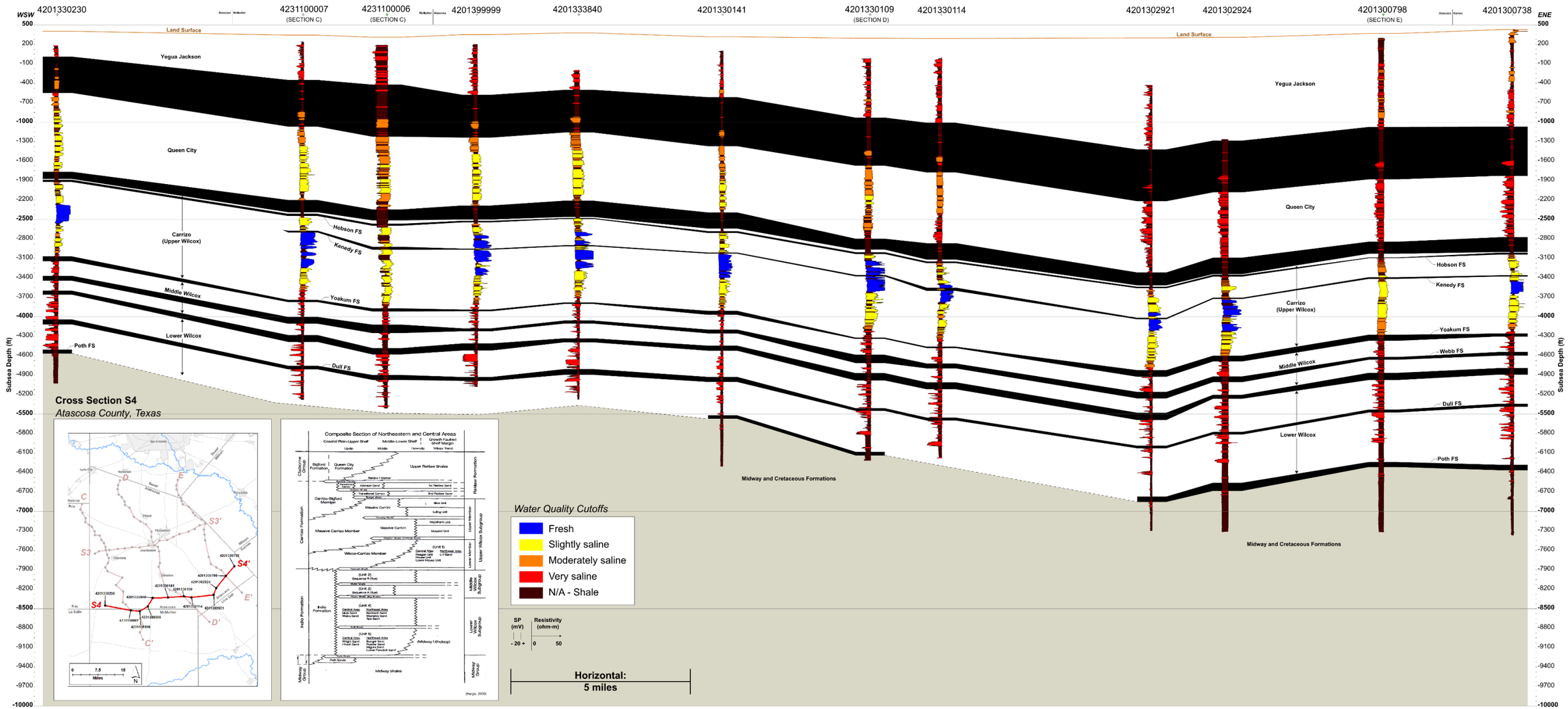

Figure 11 Strike cross-section S4 showing stratigraphy, shale locations, sand intervals, and water quality classifications at 12 log locations

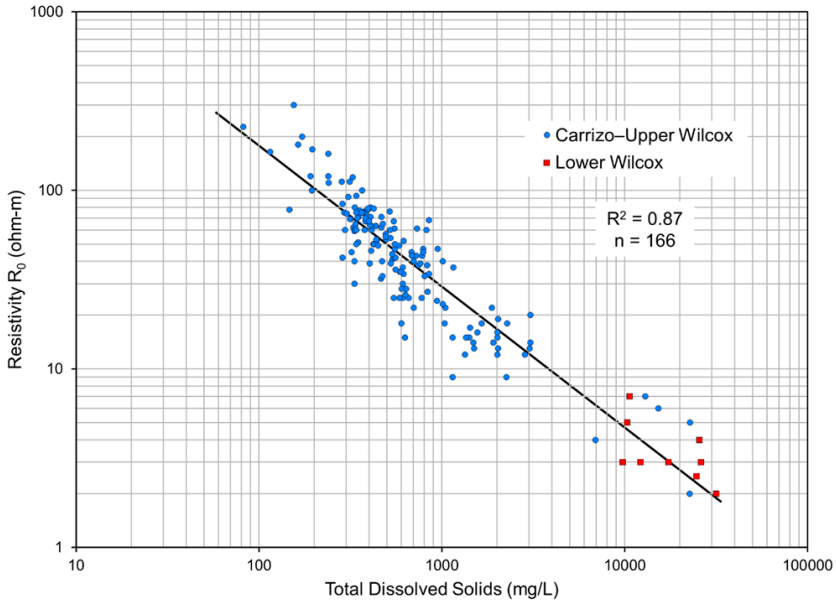

Figure 12 R_0 versus TDS concentration or the Carrizo-Upper Wilcox Aquifer in GMA 13 based on analysis of geophysical logs that are located near wells with measured TDS concentrations. (Figure copied from Hamlin and others [2016].)

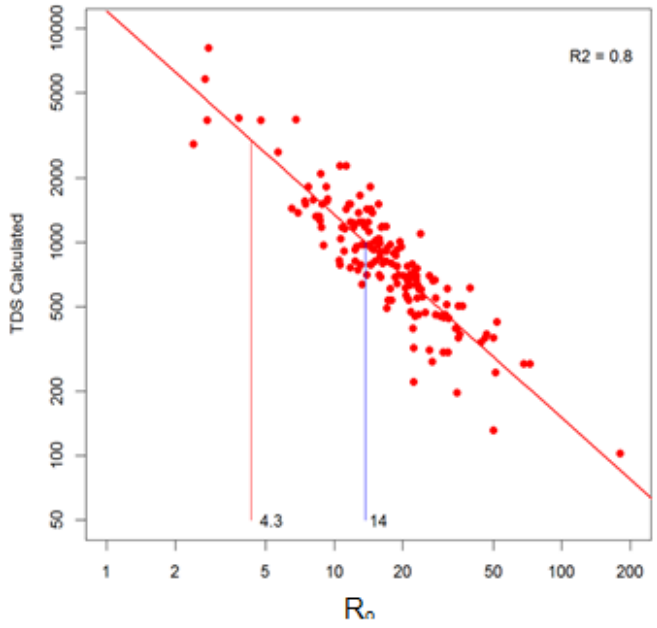

Figure 13 TDS concentration versus R_0 for the Chicot Aquifer in the Gulf Coast Aquifer System based on analysis of geophysical logs that are located near wells with measured TDS concentrations. (Figure copied from Young and others [2016].)

APPENDIX: GEOPHYSICAL WELL LOG INFORMATION

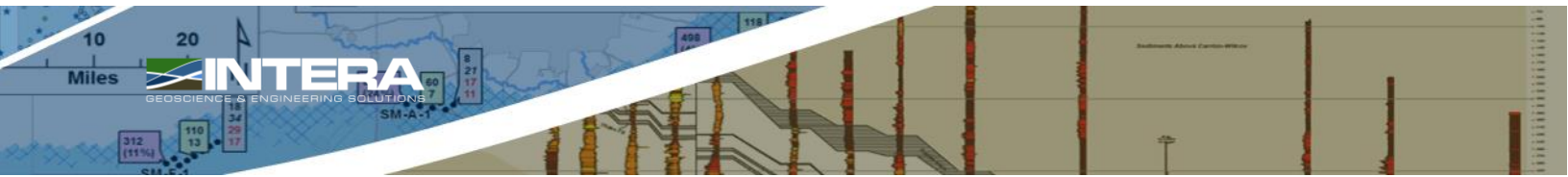

Table A-1 Location of the geophysical logs

API ID	Latitude (NAD 88)	Longitude (NAD 88)	County	Dip Section / Position	Strike Section / Position	Number of Sand Picks
4216300130	29.089053	-98.84056	Frio	C-1		17
4216300134	29.06501	98.8473011	Frio	C-2		19
4216331707	29.0505269	98.8385297	Frio	C-3		33
4216300161	29.0287133	98.8251518	Frio	C-4		28
4216300180	29.0120776	98.8263626	Frio	C-5		41
4216300220	28.9996913	98.8093399	Frio	C-6		48
4201303019	28.991663	-98.798306	Atascosa	C-7		46
HARA452A	28.972228	-98.786315	Atascosa	C-8		32
4201302535	28.956658	-98.785589	Atascosa	C-9		55
4201302500	28.954576	-98.764769	Atascosa	C-10		30
4201302595	28.935269	-98.757359	Atascosa	C-11		44
4201301729	28.922174	-98.746267	Atascosa	C-12		52
4201301577	28.9045113	98.7398778	Atascosa	C-13		53
4201301612	28.891636	-98.738127	Atascosa	C-14	S3-15	42
4201302304	28.871873	-98.732664	Atascosa	C-15		57
4201302260	28.85793	-98.725089	Atascosa	C-16		40
4201302188	28.836375	-98.72876	Atascosa	C-17		62
4201302206	28.816999	98.740719	Atascosa	C-18		60
4201302347	28.801284	-98.730653	Atascosa	C-19		74
4201331253	28.773696	-98.667346	Atascosa	C-20		85
4201331259	28.741667	-98.69444	Atascosa	C-21		52
4201333396	28.714631	-98.663359	Atascosa	C-22		65
4201302880	28.6678382	98.6659982	Atascosa	C-23		100
4201330512	28.658857	-98.652595	Atascosa	C-24		90
4231100007	28.633203	-98.631074	McMullen	C-25	S4-11	86
4231100006	28.629913	-98.592712	McMullen	C-26	S4-11	72
4231100013	28.600993	-98.589721	McMullen	C-27		113
4231134055	28.5659779	98.5766616	McMullen	C-28		83
4231133542	28.53889	-98.59167	McMullen	C-29		69
4231100016	28.50833	-98.57917	McMullen	C-30		91
HARA163A	29.190559	-98.677386	Atascosa	D-1		8
HARA140A	29.169446	-98.68656	Atascosa	D-2		12
HARA137A	29.153465	-98.687998	Atascosa	D-3		13
HARA126A	29.129631	-98.683548	Atascosa	D-4		17
HARA83A	29.118174	-98.669822	Atascosa	D-5		25
HARA80A	29.100169	-98.658324	Atascosa	D-6		24
HARA79A	29.085125	-98.655814	Atascosa	D-7		31

API ID	Latitude (NAD 88)	Longitude (NAD 88)	County	Dip Section / Position	Strike Section / Position	Number of Sand Picks
HARA75A	29.073815	-98.636243	Atascosa	D-8		36
HARA197A	29.03469	-98.618234	Atascosa	D-9		31
4201337018	29.014617	-98.590116	Atascosa	D-10		51
HARA189A	29.002812	-98.565977	Atascosa	D-11		33
4201330075	28.970741	-98.542432	Atascosa	D-12		41
HARA232A	28.948678	-98.54304	Atascosa	D-13		37
4201301771	28.912508	-98.528668	Atascosa	D-14	S3-8	87
HARA340A	28.905876	-98.514536	Atascosa	D-15		56
HARA343A	28.886226	-98.509581	Atascosa	D-16		58
4201333956	28.835971	-98.505535	Atascosa	D-17		62
4201330905	28.819977	-98.510833	Atascosa	D-18		57
4201331097	28.740495	-98.485963	Atascosa	D-19		81
4201334162	28.720892	-98.463293	Atascosa	D-20		63
4201330220	28.712089	-98.438081	Atascosa	D-21		99
4201330109	28.693011	-98.403175	Atascosa	D-22	S4-6	91
4201330113	28.664841	-98.37622	Atascosa	D-23		71
4229733497	28.5840407	98.2932115	Live Oak	D-24		76
HARB10B	29.192703	-98.429294	Bexar	E-1		22
HARB9B	29.168797	-98.435455	Bexar	E-2		24
HARB8B	29.151757	-98.434084	Bexar	E-3		24
HARB4B	29.127587	-98.425914	Bexar	E-4		38
HARA20A	29.11398	-98.414332	Atascosa	E-5		30
4201300620	29.1015606	98.4133138	Atascosa	E-6		78
HARA12A	29.087706	-98.407558	Atascosa	E-7		41
HARA10A	29.077586	-98.382385	Atascosa	E-8		39
4201332579	29.051598	-98.363285	Atascosa	E-9		54
HARA273A	29.040419	-98.354383	Atascosa	E-10		43
HARA278A	29.022998	-98.328017	Atascosa	E-11		48
4201330390	29.005363	-98.310925	Atascosa	E-12	S3-1	48
4201331058	28.979139	-98.317107	Atascosa	E-13		42
HARA300A	28.95746	-98.314159	Atascosa	E-14		45
4201300947	28.933844	-98.311509	Atascosa	E-15		102
4201300831	28.862098	-98.295846	Atascosa	E-16		126
4201333824	28.832356	-98.287493	Atascosa	E-17		102
4201332980	28.816991	-98.263384	Atascosa	E18		61
4201300804	28.80556	-98.24167	Atascosa	E19		102
4201300798	28.780795	-98.222847	Atascosa	E20		168
4229700027	28.709559	-98.153262	Live Oak	E21	S4-2	144

API ID	Latitude (NAD 88)	Longitude (NAD 88)	County	Dip Section / Position	Strike Section / Position	Number of Sand Picks
4201330390	29.005363	-98.310925	Atascosa	E-12	S3-1	48
4201330309	28.998322	-98.335262	Atascosa		S3-2	70
HARA322A	28.970526	-98.383518	Atascosa		S3-3	51
4201330868	28.961137	-98.421726	Atascosa		S3-4	48
HARA311A	28.948098	-98.448651	Atascosa		S3-5	58
HARA305A	28.935295	-98.474598	Atascosa		S3-6	36
HARA328A	28.933081	-98.507936	Atascosa		S3-7	36
4201301771	28.912508	-98.528668	Atascosa	D-14	S3-8	87
4201330161	28.911284	-98.554996	Atascosa		S3-9	60
HARA347A	28.9032	-98.592428	Atascosa		S3-10	69
4201301774	28.904152	-98.625065	Atascosa		S3-11	50
HARA439A	28.898738	-98.656879	Atascosa		S3-12	76
HARA415A	28.896479	-98.686755	Atascosa		S3-13	51
HARA424A	28.891452	-98.723266	Atascosa		S3-14	51
4201301612	28.891636	-98.738127	Atascosa	C-14	S3-15	42
HARA428A	28.886308	-98.768035	Atascosa		S3-16	53
4201302646	28.876443	-98.785541	Atascosa		S3-17	66
4201300738	28.82222	-98.18611	Atascosa		S4--1	121
4201300798	28.780795	-98.222847	Atascosa	E-21	S4--2	168
4201302924	28.72917	-98.26389	Atascosa		S4--3	101
4201302921	28.70001	-98.275	Atascosa		S4--4	159
4201330114	28.68889	-98.37083	Atascosa		S4--5	117
4201330109	28.693011	-98.403175	Atascosa	D-22	S4--6	91
4201330141	28.68889	-98.47083	Atascosa		S4--7	112
4201333840	28.686717	-98.536828	Atascosa		S4--8	110
4201399999	28.65001	-98.55833	Atascosa		S4--9	115
4231100006	28.629913	-98.592712	McMullen	C-26	S4--10	72
4231100007	28.633203	-98.631074	McMullen	C-25	S4--11	86
4201330230	28.65417	-98.74167	Atascosa		S4--12	92

Table A-2 Depth (feet) to aquifers and formations

API ID	Datum	Dip Section/ Position	Strike Section/ Position	Number of Sand Picks	GMA 13 BRACS Study	Hargis Study	Depth (Feet) to Top of Aquifers and Formations			
							Queen City Top	Carrizo / Upper Wilcox Top	Middle Wilcox Top	Lower Wilcox Top
4216300130	607	C-1		17	No	No			98	
4216300134	596	C-2		19	No	No			-78	
4216331707	636	C-3		33	No	No			-221	
4216300161	650	C-4		28	No	No			-431	
4216300180	651	C-5		41	No	No			-603	
4216300220	599	C-6		48	No	No		210	-647	
4201303019	600	C-7		46	No	Yes		139	-734	
HARA452A	611	C-8		32	No	Yes		13	-902	
4201302535	563	C-9		55	Yes	Yes		-104	-1037	-1190
4201302500	543	C-10		30	No	No		-142	-1083	
4201302595	538	C-11		44	No	Yes		-271	-1248	
4201301729	519	C-12		52	No	Yes		-369	-1371	
4201301577	521	C-13		53	No	No		-484	-1466	
4201301612	527	C-14	S3-15	42	No	Yes		-537	-1537	-1736
4201302304	489	C-15		57	No	No		-665	-1708	
4201302260	505	C-16		40	No	No		-824	-1839	
4201302188	475	C-17		62	No	No		-758	-1855	
4201302206	428	C-18		60	No	No		-876	-1910	
4201302347	431	C-19		74	No	No		-870	-1953	
4201331253	473	C-20		85	No	No	-47	-1350	-2562	-2948

API ID	Datum	Dip Section/ Position	Strike Section/ Position	Number of Sand Picks	GMA 13 BRACS Study	Hargis Study	Depth (Feet) to Top of Aquifers and Formations			
							Queen City Top	Carrizo / Upper Wilcox Top	Middle Wilcox Top	Lower Wilcox Top
4201331259	399	C-21		52	No	No		-1283	-2479	-2927
4201333396	375	C-22		65	No	No		-1615	-2859	-3270
4201302880	345	C-23		100	Yes	No	-545	-1968	-3315	-3654
4201330512	486	C-24		90	No	No	-298	-1657	-2990	-3357
4231100007	353	C-25	S4-11	86	No	No	-821	-2211	-3524	-4028
4231100006	319	C-26	S4-10	72	No	No	-946	-2293	-3814	-4181
4231100013	316	C-27		113	No	No	-1086	-2398	-4029	-4394
4231134055	372	C-28		83	No	No	-1304	-2675	-4172	-4656
4231133542	344	C-29		69	No	No	-1338	-2773	-4184	-4671
4231100016	341	C-30		91	No	No	-1445	-2848	-4229	-4760
HARA163A	672	D-1		8	No	Yes				
HARA140A	687	D-2		12	No	Yes				
HARA137A	650	D-3		13	No	Yes			547	
HARA126A	633	D-4		17	No	Yes			316	
HARA83A	631	D-5		25	No	Yes			228	
HARA80A	580	D-6		24	No	Yes			32	
HARA79A	575	D-7		31	No	Yes			-136	
HARA75A	527	D-8		36	No	Yes			-277	
HARA197A	473	D-9		31	No	Yes		127	-839	-876
4201337018	476	D-10		51	No	Yes		-114	-1005	-1118
HARA189A	474	D-11		33	No	Yes		-289	-1172	-1316

API ID	Datum	Dip Section/ Position	Strike Section/ Position	Number of Sand Picks	GMA 13 BRACS Study	Hargis Study	Depth (Feet) to Top of Aquifers and Formations			
							Queen City Top	Carrizo / Upper Wilcox Top	Middle Wilcox Top	Lower Wilcox Top
4201330075	451	D-12		41	No	Yes		-453	-1552	-1731
HARA232A	437	D-13		37	No	Yes		-551	-1722	-1889
4201301771	476	D-14	S3-8	87	No	No		-884	-2334	-2275
HARA340A	469	D-15		56	No	Yes			-2075	-2429
HARA343A	419	D-16		58	No	Yes			-2334	-2661
4201333956	350	D-17		62	No	Yes	-196	-1391	-2641	-2978
4201330905	368	D-18		57	No	No	-287	-1518	-2804	-3110
4201331097	307	D-19		81	No	No	-838	-2118	-3492	-3886
4201334162	311	D-20		63	No	No	-1018	-2323	-3732	-4107
4201330220	292	D-21		99	No	No	-1151	-2392	-3935	-4299
4201330109	295	D-22	S4-6	91	No	No	-1405	-2693	-4207	-4642
4201330113	259	D-23		71	No	No	-1633	-2978	-4483	-4964
4229733497	269	D-24		76	No	No	-2536	-3836	-5341	-5982
HARB10B	580	E-1		22	No	Yes			279	249
HARB9B	604	E-2		24	No	Yes			164	92
HARB8B	554	E-3		24	No	Yes			-9	-55
HARB4B	569	E-4		38	No	Yes		431	-323	-449
HARA20A	512	E-5		30	No	Yes		382	-527	-643
4201300620	519	E-6		78	Yes	No		243	-743	-806
HARA12A	494	E-7		41	No	Yes		102	-856	-980
HARA10A	482	E-8		39	No	Yes		-61	-1067	-1198

API ID	Datum	Dip Section/ Position	Strike Section/ Position	Number of Sand Picks	GMA 13 BRACS Study	Hargis Study	Depth (Feet) to Top of Aquifers and Formations			
							Queen City Top	Carrizo / Upper Wilcox Top	Middle Wilcox Top	Lower Wilcox Top
4201332579	465	E-9		54	No	Yes		-363	-1335	-1510
HARA273A	480	E-10		43	No	Yes		-360	-1327	-1562
HARA278A	512	E-11		48	No	Yes		-624	-1689	-1954
4201330390	415	E-12	S3-1	48	No	Yes		-828	-1958	-2226
4201331058	436	E-13		42	No	Yes		-989	-2200	-2501
HARA300A	377	E-14		45	No	Yes		-1212	-2407	-2713
4201300947	497	E-15		102	No	No	-335	-1431	-2675	-2991
4201300831	311	E-16		126	No	No	-898	-2109	-3422	-3763
4201333824	288	E-17		102	No	No	-1037	-2241	-3648	-4014
4201332980	294	E18		61	No	No	-1218	-2118	-3492	-4221
4201300804	339	E19		102	No	No	-1332	-2567	-3879	-4353
4201300798	368	E20	S4-2	168	No	Yes	-1605	-2840	-4285	-4657
4229700027	375	E21		144	No	No	-2515	-3721	-5184	-5710
4201330309	473		S3-2	70	No	Yes		-809	-1939	-2251
HARA322A	358		S3-3	51	No	Yes		-904	-2046	-2358
4201330868	361		S3-4	48	No	Yes		-911	-2021	-2338
HARA311A	398		S3-5	58	No	Yes		-904	-1984	-2313
HARA305A	443		S3-6	36	No	Yes		-888	-2000	-2323
HARA328A	414		S3-7	36	No	Yes			-1934	-2222
4201330161	450		S3-9	60	No	Yes		-782	-1868	-2150
HARA347A	501		S3-10	69	No	Yes		-723	-1752	-2058

API ID	Datum	Dip Section/ Position	Strike Section/ Position	Number of Sand Picks	GMA 13 BRACS Study	Hargis Study	Depth (Feet) to Top of Aquifers and Formations			
							Queen City Top	Carrizo / Upper Wilcox Top	Middle Wilcox Top	Lower Wilcox Top
4201301774	492		S3-11	50	No	Yes		-621	-1689	-1991
HARA439A	555		S3-12	76	No	Yes		-671	-1691	-1980
HARA415A	553		S3-13	51	No	Yes		-624	-1636	-1903
HARA424A	524		S3-14	51	No	Yes		-579	-1577	-1824
HARA428A	488		S3-16	53	No	Yes		-546	-1555	
4201302646	547		S3-17	66	No	Yes		-615	-1597	
4201300738	437		S4--1	121	No	No	-1584	-2780	-4185	-4573
4201302924	318		S4--3	101	No	No	-1821	-3100	-4605	-4985
4201302921	310		S4--4	159	No	No	-1945	-3257	-4788	-5225
4201330114	301		S4--5	117	No	No	-1507	-2861	-4365	-4767
4201330141	327		S4--7	112	No	No	-1108	-2409	-3869	-4232
4201333840	386		S4--8	110	No	No	-890	-2205	-3688	-4077
4201399999	360		S4--9	115	No	No	-959	-2277	-3798	-4195
4201330230	411		S4--12	92	No	No	-296	-1786	-3018	-3387

Table A-3 Depth to top (feet) and thickness (feet) of transgressive shales in the Wilcox Aquifer

API ID	Datum	Reklaw Shale Top	Rl Shale Top	Hb Shale Top	Hb Shale Thickness	Rn Shale Top	Rn Shale Thickness	Kn Shale Top	Kn Shale Thickness	Yk Shale Top	Yk Shale Thickness	Wb Shale Top	Wb Shale Thickness	Td Shale Top	Td Shale Thickness	Du Shale Top	Du Shale Thickness	Psh Shale Top	Psh Shale Thickness
4201300620	519	267	363									1302	14	1449	21			2217	12
4201300738	437	3217	3398	3451	22			3799	15	4708	23	4981	28	5229	36	5792	26	6719	36
4201300798	368	3208	3402	3455	7			3759	8	4712	31	5001	24	5236	23	5809	19	6608	23
4201300804	339	2906	3088	3114	9			3379	16	4374	32	4668	24	4897	33	5467	22	6261	25
4201300831	311	2431	2544	2594	18			2888	14	3788	23	4069	16	4284	25	4836	24	5683	17
4201300947	497	1928	2048	2071	24					3257	7	3460	27	3686	18	4243	19	5049	13
4201301577	521		1005											2369	14			3242	16
4201301612	527		1064									2260	3	2448	14			3419	20
4201301729	519		888											2200	17			2968	17
4201301771	476	1360	1462							2499	9	2739	12	2919	9			4086	13
4201301774	492	1113	1231							2248	12	2472	12	2630	13			3687	17
4201302188	475	1233	1280											2755	9			3651	17
4201302206	428	1304	1327											2804	9	3212		3725	25
4201302260	505	1329	1343											2764	13			3590	12
4201302304	489	1154	1177									2456		2608	13			3602	15
4201302347	431	1301	1427							2432	17	2646		2920	9	3349	13	3900	29
4201302500	543		685											1914	19			2612	10
4201302535	563	667	667									1748	5	1883	15			2543	8
4201302595	538		809											2107	19			2821	13
4201302646	547		1162									2421		2561	10			3441	13
4201302880	345	2313	2393	2435	13					3708	18	3984	15	4215	10	4697	18	5183	38
4201302921	310	3567	3788	3846	18			4327	19	5197	18	5519	15	5790	39	6299	36	7085	20
4201302924	318	3418	3639	3665	10			4025	16	4972	21	5272	31	5522	28	6110	21	6877	9
4201303019	600		461															2136	

API ID	Datum	Reklaw Shale Top	Rl Shale Top	Hb Shale Top	Hb Shale Thickness	Rn Shale Top	Rn Shale Thickness	Kn Shale Top	Kn Shale Thickness	Yk Shale Top	Yk Shale Thickness	Wb Shale Top	Wb Shale Thickness	Td Shale Top	Td Shale Thickness	Du Shale Top	Du Shale Thickness	Psh Shale Top	Psh Shale Thickness
4201330075	451	904	1040									2177	5	2326	7			3194	26
4201330109	295	2988	3225	3300	17			3657	5	4623	10	4915	21	5167	28	5702	26	6378	20
4201330113	259	3237	3452	3525	20	3619	11	3877	13	4892	16	5195	28	5445	23	5994	30		
4201330114	301	3162	3376	3449	23			3889	16	4763	18	5055	13	5313	25	5874	15		
4201330141	327	2736	2939	3008	25			3338	13	4265	28	4539	20	4786	6	5299	14	5848	20
4201330161	450	1232	1309							2355	0	2588	12	2760	13			3906	13
4201330220	292	2684	2948	2977	18			3364	13	4281	22	4569	22	4817	26	5348	v		
4201330230	411	2198	2263	2287						3506	31	3779	21	4015	15	4491		4942	28
4201330309	473	1282	1443							2455	12	2714	10	2868	9	3364		3988	17
4201330390	415	1243	1413	1472						2388	21	2622	19	2785	32	3271		3980	18
4201330512	486	2143	2252	2290	17					3554	18	3820	23	4056	13	4540		5024	30
4201330868	361	1272	1368	1394	4					2422	15	2682	17	2850	7			4038	18
4201330905	368	1886	2041	2093						3177	24	3452	27	3674	11				
4201331058	436	1425	1590	1653	7			1946		2672	20	2917	20	3094	28	3592	12	4332	18
4201331097	307	2425	2580	2623	14					3888	19	4177	16	4402	16				
4201331253	473	1823	1961	1989						3109	13	3409	12	3640	8	4136		4463	24
4201331259	399	1682	1827	1852						3021	25	3305	21	3548	21	3996		4444	21
4201332579	465	828	898									1957	18	2104	32			3093	17
4201332980	294	2704	2902	2925	12			3192	19	4199	21	4489	26						
4201333396	375	1990	2112	2120						3348	33	3628	17	3833	17	4309		4797	40
4201333824	288	2529	2723	2759	18			3057	11	3991	19	4281	21	4507	14	5065	24		
4201333840	386	2591	2780	2866	10			3284	13	4166	20	4445	18	4677	13	5066	25		
4201333956	350	1741	1906	1969						3028	27	3309	19	3518	16	4020	12	4662	16
4201334162	311	2634	2815	2909	14			3209		4107	13	4396	22	4640	26				
4201337018	476		590									1591	4	1758	4			2498	0
4201399999	360	2637	2808	2882	21			3310	13	4249	20	4540	15	4772	18	5290	20		

API ID	Datum	Reklaw Shale Top	Rl Shale Top	Hb Shale Top	Hb Shale Thickness	Rn Shale Top	Rn Shale Thickness	Kn Shale Top	Kn Shale Thickness	Yk Shale Top	Yk Shale Thickness	Wb Shale Top	Wb Shale Thickness	Td Shale Top	Td Shale Thickness	Du Shale Top	Du Shale Thickness	Psh Shale Top	Psh Shale Thickness
4216300130	607																	995	
4216300134	596																	1172	
4216300161	650																	1800	
4216300180	651																	2011	
4216300220	599		389															2062	
4216331707	636																	1436	
4229700027	375	4096	4290	4337	10			4662	11	5723	50	6065	19	6309	21	6913	44	7762	32
4229733497	269	4105	4351	4418	21	4491	15	4798	27	5901	21	6235	15	6474	19	7105	37	7854	
4231100006	319	2612	2812	2868	20			3254	16	4212	15	4485	15	4768	10	5265	10		
4231100007	353	2564	2696	2742	25			3044		4095	23	4363	18	4668	23	5114	10		
4231100013	316	2714	2963	3036	20			3408	32	4433	18	4697	13	5017	8	5464	8		
4231100016	341	3189	3418	3502	21	3585	19	3820	22	4699	16	5088	13	5382	15	5790	15	6370	26
4231133542	344	3117	3317	3426	18			3775	23	4655	20	5012	3	5322	10	5735	13	6168	17
4231134055	372	3047	3264	3358	18	3447	12	3732	27	4650	26	5013	15	5290	27	5767	18	6297	21
HARA10A	482	543	630									1666	14	1806	30			2684	21
HARA126A	633																	905	
HARA12A	494	392	474									1455	19	1607	28			2378	18
HARA137A	650																	669	
HARA140A	687																	646	
HARA163A	672																	563	
HARA189A	474		763									1788	2	1938	9			2741	15
HARA197A	473	346	350									1349	-2	1508	9			2198	10
HARA20A	512	130	191									1139	16	1283	41			1973	14
HARA232A	437	988	1121									2319	7	2490	9			3440	15
HARA273A	480	840	945							1818	11	2026	16	2170	30			3197	18
HARA278A	512	1136	1293							2229	18	2443	23	2597	28			3545	21

API ID	Datum	Reklaw Shale Top	Rl Shale Top	Hb Shale Top	Hb Shale Thickness	Rn Shale Top	Rn Shale Thickness	Kn Shale Top	Kn Shale Thickness	Yk Shale Top	Yk Shale Thickness	Wb Shale Top	Wb Shale Thickness	Td Shale Top	Td Shale Thickness	Du Shale Top	Du Shale Thickness	Psh Shale Top	Psh Shale Thickness
HARA300A	377	1589	1728	1743	18					2817	20	3080	10	3252	18	3768	19	4593	26
HARA305A	443	1331	1445							2504	10	2755	12	2923	14			4129	17
HARA311A	398	1302	1417							2441	13	2701	10	2871	14			4092	20
HARA322A	358	1262	1415							2455	10	2706	10	2870	15			4028	15
HARA328A	414	1258	1371							2391	15	2623	13	2793	12				
HARA340A	469		1547							2627	13	2884	14	3059	8			4273	15
HARA343A	419		1704							2801	18	3066	14	3252	11			4475	18
HARA347A	501	1224	1278							2315	5	2547	12	2722	9			3789	17
HARA415A	553	1177	1242									2446	10	2609	13			3640	12
HARA424A	524		1103									2348	-3	2506	10			3462	13
HARA428A	488		1034									2295		2446	12			3340	15
HARA439A	555	1226	1281							2246	12	2525	10	2690	9			3726	16
HARA452A	611		598											1780	12			2404	17
HARA75A	527													1042	13			1579	7
HARA79A	575													893	19			1378	9
HARA80A	580													705	20			1204	
HARA83A	631													590				1070	
HARB10B	580											331	7	458	4			959	9
HARB4B	569		138									1004	14	1158	28			1801	7
HARB8B	554											607	2	749	16			1302	5
HARB9B	604											503	9	636	9			1226	7